



AFRL-AFOSR-VA-TR-2015-0241

DARPA) OPTICAL RADIATION COOLING AND HEATING IN INTEGRATED DEVICES

**Hong Tang
YALE UNIV NEW HAVEN CT**

**07/21/2015
Final Report**

DISTRIBUTION A: Distribution approved for public release.

**Air Force Research Laboratory
AF Office Of Scientific Research (AFOSR)/ RTB
Arlington, Virginia 22203
Air Force Materiel Command**

REPORT DOCUMENTATION PAGE				<i>Form Approved</i> OMB No. 0704-0188	
<small>The public reporting burden for this collection of information is estimated to average 1 hour per response, including the time for reviewing instructions, searching existing data sources, gathering and maintaining the data needed, and completing and reviewing the collection of information. Send comments regarding this burden estimate or any other aspect of this collection of information, including suggestions for reducing the burden, to the Department of Defense, Executive Service Directorate (0704-0188). Respondents should be aware that notwithstanding any other provision of law, no person shall be subject to any penalty for failing to comply with a collection of information if it does not display a currently valid OMB control number.</small>					
PLEASE DO NOT RETURN YOUR FORM TO THE ABOVE ORGANIZATION.					
1. REPORT DATE (DD-MM-YYYY) 07/16/2015		2. REPORT TYPE Final		3. DATES COVERED (From - To) June 15, 2010 - June 14, 2015	
4. TITLE AND SUBTITLE DARPA OPTICAL RADIATION COOLING AND HEATING IN INTEGRATED DEVICES				5a. CONTRACT NUMBER	
				5b. GRANT NUMBER FA9550-10-1-0297	
				5c. PROGRAM ELEMENT NUMBER	
6. AUTHOR(S) Hong Tang Chee-Wei Wong				5d. PROJECT NUMBER	
				5e. TASK NUMBER	
				5f. WORK UNIT NUMBER	
7. PERFORMING ORGANIZATION NAME(S) AND ADDRESS(ES) Yale University, 15 Prospect St, New Haven CT 06511 Columbia University, 500 West 120th St, New York NY 10027				8. PERFORMING ORGANIZATION REPORT NUMBER	
9. SPONSORING/MONITORING AGENCY NAME(S) AND ADDRESS(ES) DARPA ORCHID through AFOSR				10. SPONSOR/MONITOR'S ACRONYM(S) AFOSR	
				11. SPONSOR/MONITOR'S REPORT NUMBER(S)	
12. DISTRIBUTION/AVAILABILITY STATEMENT For public release					
13. SUPPLEMENTARY NOTES					
14. ABSTRACT <p>In this DARPA's ORCHID program, Yale/Columbia's team focuses on chip-scale optomechanics with emphasis on circuit integration on silicon platforms.</p> <p>In Phase I (06/2010-06/2012), we advanced the-state-of-art cavity optomechanical devices with performance parameters exceeding DARPA's specifications. Selected high performance devices are optimized for specific applications: (1) low-noise optomechanical oscillators; (2) femtogram optomechanical cavities for sensing; (3) strong optomechanical backaction and coherent control for quantum transducers.</p> <p>In Phase II (07/2012-06/2015), we added electronic control in Cavity Optomechanics and developed a number of cavity electro-optomechanical systems for realizing strong coupling between photon, phonon and microwave fields. These cavity electro-optomechanical systems were fabricated</p>					
15. SUBJECT TERMS optomechanics, MEMS, oscillator, integrated photonics, cavity optomechanics					
16. SECURITY CLASSIFICATION OF:			17. LIMITATION OF ABSTRACT UU	18. NUMBER OF PAGES 37	19a. NAME OF RESPONSIBLE PERSON Hong Tang
a. REPORT unclassified	b. ABSTRACT unclassified	c. THIS PAGE unclassified			19b. TELEPHONE NUMBER (Include area code) 203-432-4256

INSTRUCTIONS FOR COMPLETING SF 298

1. REPORT DATE. Full publication date, including day, month, if available. Must cite at least the year and be Year 2000 compliant, e.g. 30-06-1998; xx-06-1998; xx-xx-1998.

2. REPORT TYPE. State the type of report, such as final, technical, interim, memorandum, master's thesis, progress, quarterly, research, special, group study, etc.

3. DATES COVERED. Indicate the time during which the work was performed and the report was written, e.g., Jun 1997 - Jun 1998; 1-10 Jun 1996; May - Nov 1998; Nov 1998.

4. TITLE. Enter title and subtitle with volume number and part number, if applicable. On classified documents, enter the title classification in parentheses.

5a. CONTRACT NUMBER. Enter all contract numbers as they appear in the report, e.g. F33615-86-C-5169.

5b. GRANT NUMBER. Enter all grant numbers as they appear in the report, e.g. AFOSR-82-1234.

5c. PROGRAM ELEMENT NUMBER. Enter all program element numbers as they appear in the report, e.g. 61101A.

5d. PROJECT NUMBER. Enter all project numbers as they appear in the report, e.g. 1F665702D1257; ILIR.

5e. TASK NUMBER. Enter all task numbers as they appear in the report, e.g. 05; RF0330201; T4112.

5f. WORK UNIT NUMBER. Enter all work unit numbers as they appear in the report, e.g. 001; AFAPL30480105.

6. AUTHOR(S). Enter name(s) of person(s) responsible for writing the report, performing the research, or credited with the content of the report. The form of entry is the last name, first name, middle initial, and additional qualifiers separated by commas, e.g. Smith, Richard, J, Jr.

7. PERFORMING ORGANIZATION NAME(S) AND ADDRESS(ES). Self-explanatory.

8. PERFORMING ORGANIZATION REPORT NUMBER. Enter all unique alphanumeric report numbers assigned by the performing organization, e.g. BRL-1234; AFWL-TR-85-4017-Vol-21-PT-2.

9. SPONSORING/MONITORING AGENCY NAME(S) AND ADDRESS(ES). Enter the name and address of the organization(s) financially responsible for and monitoring the work.

10. SPONSOR/MONITOR'S ACRONYM(S). Enter, if available, e.g. BRL, ARDEC, NADC.

11. SPONSOR/MONITOR'S REPORT NUMBER(S). Enter report number as assigned by the sponsoring/monitoring agency, if available, e.g. BRL-TR-829; -215.

12. DISTRIBUTION/AVAILABILITY STATEMENT. Use agency-mandated availability statements to indicate the public availability or distribution limitations of the report. If additional limitations/ restrictions or special markings are indicated, follow agency authorization procedures, e.g. RD/FRD, PROPIN, ITAR, etc. Include copyright information.

13. SUPPLEMENTARY NOTES. Enter information not included elsewhere such as: prepared in cooperation with; translation of; report supersedes; old edition number, etc.

14. ABSTRACT. A brief (approximately 200 words) factual summary of the most significant information.

15. SUBJECT TERMS. Key words or phrases identifying major concepts in the report.

16. SECURITY CLASSIFICATION. Enter security classification in accordance with security classification regulations, e.g. U, C, S, etc. If this form contains classified information, stamp classification level on the top and bottom of this page.

17. LIMITATION OF ABSTRACT. This block must be completed to assign a distribution limitation to the abstract. Enter UU (Unclassified Unlimited) or SAR (Same as Report). An entry in this block is necessary if the abstract is to be limited.

**DARPA) OPTICAL RADIATION COOLING AND HEATING IN INTEGRATED
DEVICES**

DARPA ORCHID Final Report

“Circuit cavity optomechanics for cooling and amplification on a silicon chip”

PI: Hong Tang, Yale University; co-PI: Chee-Wei Wong, Columbia University

Grant No: FA9550-10-1-0297

Reporting period: 06/15/2010-06/14/2015

Date submitted: 07/13/2015

Table of Contents

1. Summary of notable accomplishments	3
2. Phase I efforts on device advancements	5
2.1. Device performance – comparing milestones and results.....	5
2.2. Advancing optomechanics from MHz to GHz	7
2.3. Device scaling to femtograms.....	9
2.4. Cavity optomechanics in high amplitude regime.....	10
2.5. Investigation of fundamental phase noise of very high Q SiN nanomechanical resonators.	12
2.6. What did not work in Phase I.....	12
2.7. What have we learned from phase I.....	13
3. Summary of Phase II efforts: cavity electro-optomechanics and cavity piezo-optomechanics	13
3.1. From cavity optomechanics to cavity electro-optomechanics	13
3.2. Silicon cavity electro-optomechanics: advancing to SHF operation	14
3.3. SiN electro-optomechanics: 15dB thermal noise squeezing.....	15
3.4. AlN piezo-optomechanical system.	17
3.5. Development of the first s-band AlN 1D piezo-optomechanical cavity	19
3.6. Development of X-band piezo-optomechanical oscillator.....	20
3.7. A 10.5GHz piezo-optomechanical oscillator	22
3.8. Packaging of optomechanical oscillator.....	24
3.9. Parametric optomechanical oscillations in 2D slot-type high-Q PhC cavities and feedback and harmonic locking for low-noise reference clocks	24
3.10. CMOS monolithically integrated optomechanical resonators	25
3.11. Phase noise measurement of monolithic OMO.....	27
4. Other accomplishments of fundamental interests	29
4.1. Photonic Bus Synchronization of Remote Nanomechanical Oscillators	29
4.2. Dynamic dissipative cooling of strong-coupled mechanical oscillator and coupled cavities	31
4.3. “Phonon” radiation pressure force and cascaded optomechanical transparency	31
Appendix.....	34
Appendix 1. Yale/Columbia team publication list (as of 07/06/2015)	34
Appendix 2. Supported postdoc/graduate students	36
Appendix 3. Honors received by supported postdoc/graduate students.....	37

1. Summary of notable accomplishments

In this DARPA's ORCHID program, Yale/Columbia's team focuses on chip-scale optomechanics with emphasis on circuit integration on silicon platforms.

In Phase I (06/2010-06/2012), we advanced the-state-of-art cavity optomechanical devices with performance parameters exceeding DARPA's specifications. Selected high performance devices are optimized for specific applications: (1) low-noise optomechanical oscillators; (2) femtogram optomechanical cavities for sensing; (3) strong optomechanical backaction and coherent control for quantum transducers.

In Phase II (07/2012-06/2015), we added electronic control in Cavity Optomechanics and developed a number of cavity electro-optomechanical systems for realizing strong coupling between photon, phonon and microwave fields. These cavity electro-optomechanical systems were fabricated from three different material systems – Si, SiN and AlN. The latter two substrate systems were first designed by our team and now become very popular in Optomechanics community. Particular to the silicon platform, we developed a post-CMOS process which allowed the interrogation of Optomechanics on a CMOS platform with integrated Germanium detectors. The most notable accomplishments we have made in Phase II include: (1) The development of AlN-on-silicon platform for cavity electro-optomechanics and nonlinear optics; (2) Development of X-band optomechanical oscillators; (3) Discovery of phonon “radiation pressure” in optomechanical resonators; (4) Demonstration of coherent control of cavity electro-mechanical resonators; (5) Non-volatile optomechanical switches and memory; (6) Photonic synchronization of two coupled resonators.

Our program also trained a number of outstanding researchers. At Yale, four postdoc members working on this project secured faculty jobs: Mo Li (University of Minnesota), Wolfram Pernice (Karlsruhe Institute of Technology, Germany), Harish Bhaskaran (Oxford University, UK), Xiankai Sun (Chinese University of Hong Kong). Two postdoctoral researchers became research scientist or junior group leader at national labs: Mahmood Bagheri (JPL/NASA) and Daniel Garcia-Sanchez (Institute of Nanosceince, Paris). The program also supported four Ph.D. students: Xiong Chi (now postdoc at IBM), Kingyan Fong (now postdoc at Berkeley), Linran Fan, Xu Han. Two of graduate students were awarded best presentation awards at international conferences. Similarly at Columbia, we also have great outcome in training postdocs and graduate students.

Throughout this program, we published 48 journal papers, gave 80+ invited talks/seminars, and contributed to 40+ conference proceedings. A full list of papers we published in this period can be found in Appendix I. Below we provide a highlight of most notable results.

- Advance of device technology
 - Optomechanics with record low mass of 25fg. [Sun et al, Nano Letter, 2012]
 - Optomechanics with record high frequency: 10.3 GHz. [Xu et al, APL 2015]
 - On-chip sensitivity $6.2 \times 10^{-18} \text{m}/\sqrt{\text{Hz}}$. [Sun et al, APL 2012]

- Optomechanical amorphous crystal with high optical Q: 7.4×10^5 . [Zhang et al, Opt. Lett. 2012]
- Optomechanical resonator with high room temperature mechanical Q: 2.5×10^6 [Fong et al, PRB 2012]
- Optomechanical cavity with very large transduction [Li et al, OE 2010, Zheng et al, APL 2012, Luan et al Sci. Rep. 2014],
- New backaction physics: amplification, cooling and squeezing
 - Parametric noise squeezing of an electro-optomechanical resonator [Poot et al, APL 2014, Poot et al, NJP 2014]
 - High amplitude NEMS and nonlinear optomechanics (Bagheri, Nature Nanotech 2011)
 - Dissipative cooling dynamics, [Liu et al, PRL 2013]
 - Coupled cavity cooling, [Liu et al, PRA 2015]
 - Microwave assisted amplification [Fong et al, PRA 2014]
 - Synchronization of two remote optomechanical oscillators and injection locked optomechanical arrays (Bagheri, PRL 2013)
 - Optomechanical anti-damping in fluid (Fong et al, Nano Lett. in review 2015)
 - Phase noise theory of optomechanical oscillators (Fong et al PRA 2014)
 - Cascaded optical transparency in multimode-cavity optomechanical systems (Fan et al, Nature Communications).
- New material and device system
 - HS(SiN)-on-oxide and AlN-on-oxide platforms [Fong et al, Optics Express 2011, Xiong et al, APL 2012]
 - Cavity electro-optomechanics and cavity piezo-optomechanics [Xiong et al, NJP 2012, Sun et al, APL 2012, Xiong et al, APL 2013, Fan et al, APL 2013]
 - Hybrid superconducting – optomechanical system
 - CMOS integrated cavity Optomechanics [Sun et al, Optics Letters 2014]
 - Ge integrated cavity optomechanical oscillators [Luan et al, Sci. Rep 2014]
- Device applications
 - Low phase noise oscillator (30MHz-> 3GHz-> 3GHz -> 8.3GHz -> 10.3GHz) (Xiong et al, APL 2012, Xu et al, NJP 2014).
 - Low noise integrated oscillator (Luan et al, Sci. Rep 2014)
 - Feedback and harmonic locking (Zheng et al, APL 2013)
 - Control elements for integrated photonics: phase shifters, switches (Poot et al, APL 2014)
 - Optomechanical resonator in microfluid of aqueous environment (Fong et al, Nano Lett, in review 2015)

2. Phase I efforts on device advancements

2.1. Device performance – (original) milestones and results

Proposed Device A: Radial contour resonator in 2D PHC cavity: $Q_{opt} = 4.10^4$, $Freq = 1.5$ GHz, $mass = 3.2$ pg; $Q_{mech} = 10^4$, $Z = 10^{-9}$

The Z parameter for this originally proposed device was far exceeded. In our final device (sunflower structure), the optical Q is 7.4×10^5 (20x better than milestone). The frequency is 2.2GHz and resonator mass is 0.89pg, both exceeding their respective milestones. The mechanical quality factor varies from 70 to 4000 in air at room temperature, a bit lower than target value. Yet, even if we take the lowest mechanical Q of 70, the Z parameter is already 0.7×10^{-6} , approaching the original phase II Z-parameter milestone. The sunflower optomechanical structures are probably the mostly engineered optomechanical devices. The design involves simultaneous optimization more than 8 device parameters: lattice constant, filling factor, gap, disk radius, input waveguide termination, width, number of circular lattices, and photonic crystal termination. From optics point of view, for the first time, we are able to achieve wavelength-size whispering gallery mode resonator with high quality factors on the order of million. The mechanical design also went through many iterations to produce the most suitable mechanical suspension for the crystal and the resonating disk. The proposed and realized structures are shown in the figure below. Our simulation shows that the device's mechanical Quality factor is currently limited by the clamping due to the pedestal.

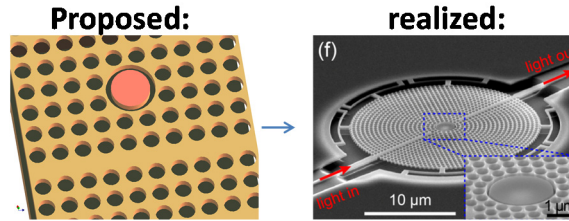


Fig.1, Device A: proposed and realized

Proposed Device B: Beam resonator in 2D PHC cavity: $Q_{opt} = 2.10^4$, $Freq = 0.5$ GHz, $mass = 160$ fg; $Q_{mech} = 10^4$, $Z = 10^{-9}$

The parameters for this proposed device were achieved and exceeded. Particularly in this Columbia-Yale work, a series of femtogram optomechanical cavities were successfully designed, fabricated and tested. For example, device B1 design has $Q_{opt} = 105,000$, $freq = 0.69$ GHz, $mass = 20$ fg; $Q_{mech} = 49,900$; device B2 has $Q_{opt} = 95,000$, $freq = 0.60$ GHz, $mass = 16$ fg; $Q_{mech} = 203,000$. The designs were performed with full FDTD intensive computations for the optical designs (including optimizing the band structure, spectral location of the localized mode, radiation suppression, optical gradient force design, etc) and three-dimensional finite-element designs for the mechanical design (including interference of the elastic waves for energy localization and high mechanical Q, etc). The devices were fabricated in silicon-on-insulator, demonstrating 1-GHz fundamental flexural modes, 25 fg masses and $0.94 \text{ fm/Hz}^{1/2}$ displacement sensitivities. The

measured intrinsic optical Q is up to 52,000 and matches the designs very well; the measured mechanical Q_{mech} is 1200 at room temperature, about 10x less than the designed value. At low temperature, the quality factor will be significantly higher. The Z parameter is 1.5×10^{-9} for device shown in the figure above. The uniqueness of this device is their ultra-low mass.

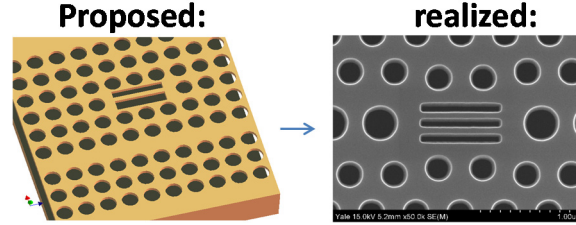


Fig. 2, Device B: proposed and realized

Proposed Device C: Dumbbell-slot resonator in PHC cavity: $Q_{\text{opt}} = 3 \cdot 10^4$, $\text{Freq} = 1.0 \text{ GHz}$, $\text{mass} = 110 \text{ fg}$; $Q_{\text{mech}} = 10^4$, $Z = 10^{-9}$

We have achieved most of the proposed device parameters including DARPA's Z parameter. For example, device C1 has $Q_{\text{opt}} = 150,000$, $\text{Freq} = 1.6 \text{ GHz}$, $\text{mass} = 20 \text{ fg}$, $Q_{\text{mech}} = 10^3$, $Z = 3 \times 10^{-6}$. (Fig. 3). The idea was to build the smallest cavity possible which comprises of a 1D photonic crystal beam cavity with a longitudinal slot in the cavity to form mechanical resonator. The devices perform well from milestone point of view. However we have found that this class of 1D photonic crystal structures has limited power handling capability. When the cavity photon number is high, the cavity becomes unstable and difficult to be cooled to low temperature. We therefore did not pursue the cooling and backaction with this type of devices. In its place we experimented on Device D below and the microwheel/microdisk devices during phase II.

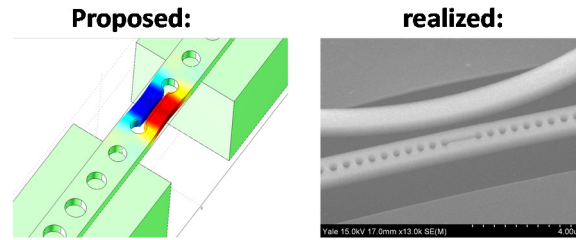


Fig. 3, Device C: proposed and realized

Proposed Device D: ultrahigh Q/V slot type photonic crystal cavities: $Q_{\text{opt}} = 5 \cdot 10^6$, $\text{Freq} = 460 \text{ MHz}$, $Q_{\text{mech}} = 10^4$, $Z = 10^{-6}$

The design, device images and measurement results of high Q/V slot cavity are shown in Fig. 4. In this cavity we reached very high Z parameters and realized the strong optomechanical dynamical interactions in ultrahigh Q/V slot-type photonic crystal cavities. The dispersive coupling is based on mode-gap photonic crystal cavities with light localization in an air mode [Fig. 4(a)-(e)] with $0.02(\lambda/n)^3$ modal volumes while preserving optical cavity Q up to 5×10^6 [Fig. 4(f)-(i)]. The mechanical mode is modeled to have fundamental resonance $Q_m/2\pi$ of 460 MHz and a quality factor Q_m estimated at 12,000 [Fig. 4(j)-(k)]. For this slot-type optomechanical cavity, the dispersive coupling g_{om} is numerically computed at up to 940 GHz/nm (L_{om} of 202 nm) for the

fundamental optomechanical mode [Fig. 4(l)]. Dynamical parametric oscillations for both cooling and amplification, in the resolved and unresolved sideband limit, are examined numerically, along with the displacement spectral density and cooling rates for various operating parameters.

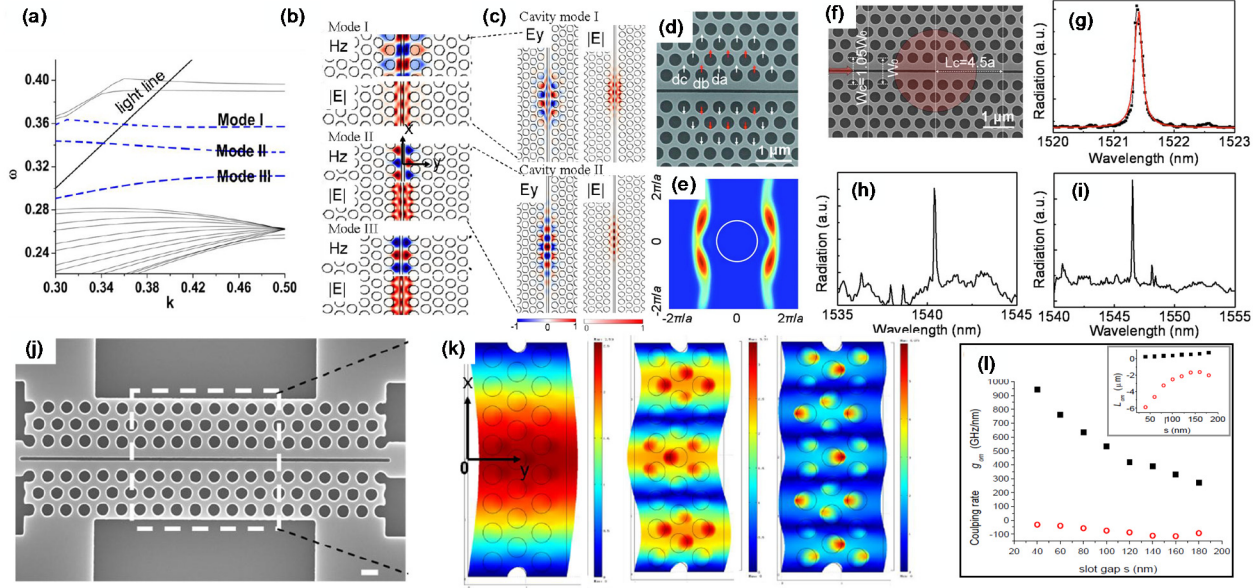


Fig. 4. The design and first numerically and experimentally demonstrations for the ultrahigh-Q/V optomechanical cavity.

2.2. Advancing optomechanics from MHz to GHz

Obtaining high frequencies in optomechanical resonators is desirable for developing high-speed systems for sensing and wavelength-selective signal routing. It also relieves the cooling requirement for reaching ground state of mechanical resonators. To move to high frequencies, one can take two approaches: 1) Scaling the mechanical resonators to smaller dimensions; 2) Use stiff bulk resonant modes. In Section 2.3, we will describe our effort on device scaling to achieve high frequency resonances. However smaller devices also have less power handling capability, the transduction efficiency also goes down. Therefore device scaling has its own limits. In this section, we describe our approaches on developing bulk mode resonators.

Our bulk-mode resonators are based upon radial-contour modes of disks and rings. The wheel resonators were designed with the two guidelines: (i) to minimize the anchor loss to the substrate, the spoke length should be an odd multiple of a quarter wavelength of the spoke's longitudinal mode; (ii) to minimize the energy loss from the vibrating ring to the spokes, the attaching point should be at a nodal point of the targeted mode. This kind of micro-wheel/microdisk resonator structures were not in our original milestones but they have displayed excellent optomechanical performances.

This group of resonators have allowed us to reach very high resonant frequencies, low phase noise, and high transduction sensitivities. In Phase I, we developed processes to fabricate

microwheel resonators in three different materials: Si, SiN and AlN. They all reached the Z-parameter milestones. For example, Device D1 (made of Silicon) has $Q_{\text{opt}} = 1 \times 10^6$, $\text{freq} = 1.5\text{GHz}$, $\text{mass} = 78\text{pg}$, $Q_{\text{mech}} = 3900$, and $Z = 1.2 \times 10^{-9}$; Device D2 (made of Stoichiometric Silicon Nitride) has $Q_{\text{opt}} = 1.5 \times 10^6$, $\text{freq} = 190\text{MHz}$, $\text{mass} = 87\text{pg}$, $Q_{\text{mech}} = 4000$, and $Z = 1.1 \times 10^{-9}$; Device D3 (made of Aluminum Nitride) has $Q_{\text{opt}} = 0.5 \times 10^6$, $\text{freq} = 1.04\text{GHz}$, $\text{mass} = 420\text{pg}$, $Q_{\text{mech}} = 2500$, and $Z = 1.1 \times 10^{-9}$. As a result of high optomechanical transduction coefficients, all these devices all have reached attometer displacement sensitivity. For instance, the AlN wheel has a displacement sensitivity of $6.2 \times 10^{-18}\text{m/rHz}$ sensitivity for its 2nd radial contour mode. These wheel structures are very robust and less sensitive to environment perturbations therefore are promising for device applications. For example, the D1 device is currently being investigated for gas sensing. D2 device is now packaged in microfluidic channel to operate in water. We found that the optomechanical amplification can counter fluidic damping and allow the device to self-oscillate in water. The D3 device on the other hand, is made of AlN and enables very low phase noise oscillator operating at GHz carrier frequencies.

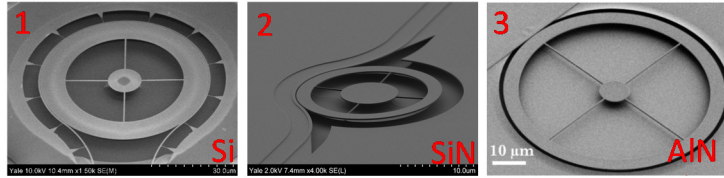


Fig. 5, Device D: microwheel resonators

The devices were first characterized optically. The measured free spectral ranges of the wheel and disk resonators are 3.39 nm and 22.5 nm, respectively. The loaded optical Q 's are above 500,000 for wheels and about 70,000 for disks, corresponding to finesse of 1112 and 1020, respectively. The mechanical modes were measured by tuning the input laser wavelength to the maximum slope of an optical resonance and recording the noise spectrum of the optical transmission. The laser intensity was kept low enough that the backaction is negligible and thus the measured mechanical Q 's do not change and reflect the intrinsic values.

Figure 6 shows the examples of RF spectra of the mechanical modes of the wheel and disk resonators measured in air. The dominating modes in Fig. 6(a) and the three peaks in Fig. 6(f) are identified by FEM simulation. The weaker peaks around the dominating ones in Fig. 6(a) are attributed to the higher-order azimuthal wheel modes because the spokes break the perfect circular symmetry of the ring. The mechanical Q 's are closely related to their modal profiles. The fundamental modes [Figs. 6(b) and 6(g)] possess lower Q factors than the higher-order modes. This can be attributed to the fact that the fundamental modes are radial breathing modes and thus experience larger viscous damping from the air because of the large collective radial motion. The higher-order modes are more immune to this type of loss because of their relative motions inside the resonators.

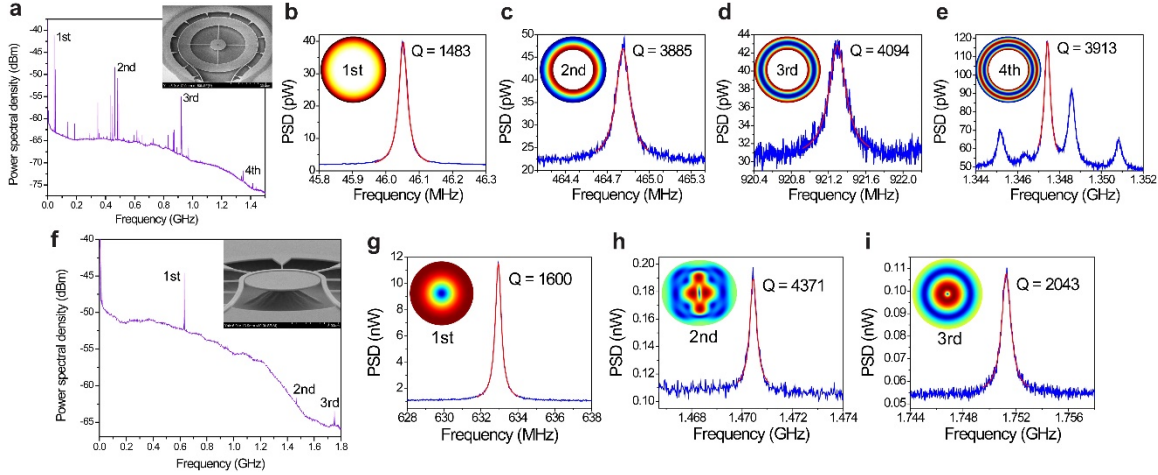


FIG 6. a) Full-range RF power spectral density (PSD) of the wheel resonator (top panels) and microdisk resonators (bottom panels).

In terms of mechanical frequency, these devices can be operated anywhere between 50MHz and 2GHz, depending on the designed device geometries. Our goal of reaching GHz optomechanical resonators were clearly demonstrated in these devices.

2.3. Device scaling to femtograms

One of our program goals is to push the scaling limit and create nanomechanical resonators with ultra-small mass. Ultrasmall-mass resonators are particularly desirable because they inherently operate at ultrahigh frequency of the fundamental mechanical mode, which has advantage for developing high-speed sensors with ultimate mass sensitivity. Throughout the program, we exercised the idea of “nanobeam-in-cavity” at the nanoscale, by embedding a doubly-clamped nanomechanical beam in a two-dimensional (2D) photonic crystal (PhC) nanocavity. The use of 2D photonic crystals improves the power handling capabilities comparing to the 1D photonic crystal nanocavities. The simplest approach to realize nanobeam-in-cavity is to directly enclose a tiny nanomechanical resonator within the well-established photonic crystal L3 cavity. However, due to the strong perturbation to the cavity mode by the embedded nanobeams, the PhC nanocavity had to be thoroughly redesigned and engineered to ensure maximum confinement of the cavity mode. Careful optimization of the cavity mode results in a high loaded experimental optical Q of 10,000. Thanks to the well-defined geometry and ultrasmall size (~ 25 fg) of the nanomechanical resonator, optical transduction of the nanobeams’ fundamental mechanical flexural mode around 1 GHz was performed. The room temperature mechanical Q was measured to be 1230 in vacuum and 580 in air.

In the demonstrated devices, the mechanical modal volume is less than 1/7 of the optical cavity modal volume. The optimized devices were fabricated from standard SOI substrates (220-nm Si on 3- μ m buried oxide), as shown in Fig. 7a and b. Fig. 7c-f shows the simulated optical modes and mechanical mode. In experiment, a single mechanical mode at 903.6 MHz is observed in the entire spectrum range, which is considered to be the differential mode because of its dominantly stronger optomechanical coupling to the optical cavity mode. The common mode is not observed due to its

weak coupling to the optical mode, and also probably stronger optomechanical damping comparing to the differential mode.

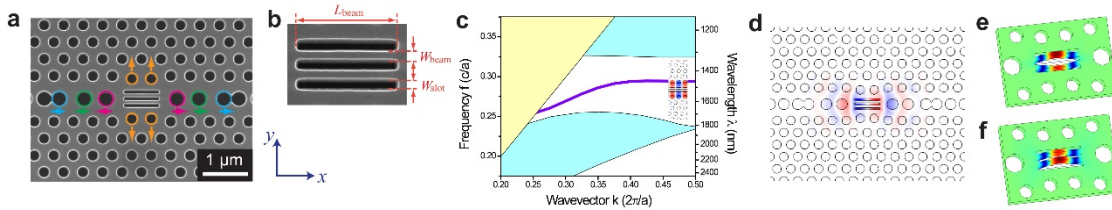


Fig.7. Femtogram “beam-in-PhC” nanomechanical resonator: device and simulations

2.4. Cavity optomechanics in high amplitude regime.

In this part of work, we theoretically and experimentally investigate the maximum amplitude of mechanical oscillators coupled to optical cavities. Reaching high amplitude is important for oscillator operation because higher amplitudes imply lower impact of thermal energy to the phase noise. The optical backaction on the resonator enables self-sustained oscillations whose limit cycle is set by the cavity dynamic range. The maximum attainable amplitude and also the quantum efficiency of the backaction process are studied for both unresolved and resolved cavities. Quantum efficiencies largely exceeding one are found in the resolved sideband regime, whereas the maximum amplitude is found in the unresolved system. The main focus of this work is the role of the cavity, but the question of how mechanical nonlinearities affect the maximum amplitude has been also addressed.

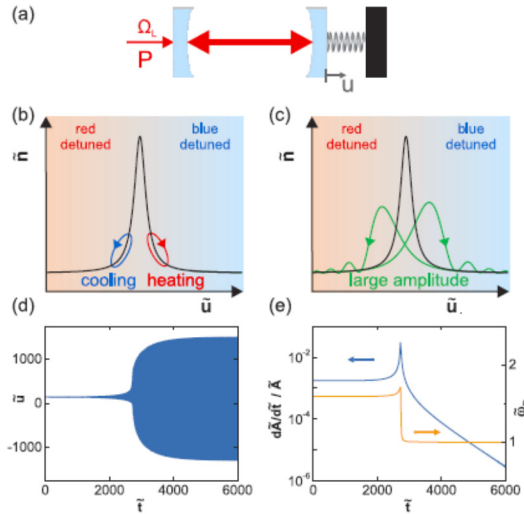


Figure 8. Backaction limits of high amplitude nanomechanical resonators

Our results indicate that above the threshold self-sustained oscillations grow until the resonator reaches a limit cycle set by the dynamic range of the cavity. The largest amplitudes are obtained with an unresolved cavity, but the largest quantum efficiencies are found in the resolved case. The latter can be much larger than one because many sidebands are involved, resulting in multi-phonon

emission. For large amplitudes the motion is anharmonic, and numerical simulations show that the final amplitude is insensitive to the cavity detuning and linewidth. Mechanical nonlinearities only have a modest effect in the unresolved sideband regime, whereas in the resolved case the shift in oscillation frequency due to anharmonicities can have a strong effect on the amplitude. (Fig. 8)

Experimentally we use a bistable nanomechanical resonator with two stable states to demonstrate coherent amplification and switching of nanomechanical resonators by optical cooling and amplification. (Fig. 9a) The dynamic manipulation by optical backaction drives nanomechanical resonators at high amplitudes. A non-volatile memory is also demonstrated. The nano-mechanical resonators used for this study are fabricated on a 110nm-thick SOI wafer. Due to residual compressive stress introduced by the SOI wafer bonding process, free-standing doubly clamped beams are slightly buckled and show bi-stable behavior; the mechanical resonator has two stable configurations at rest, buckled up and buckled down (see Fig. 9(a)).

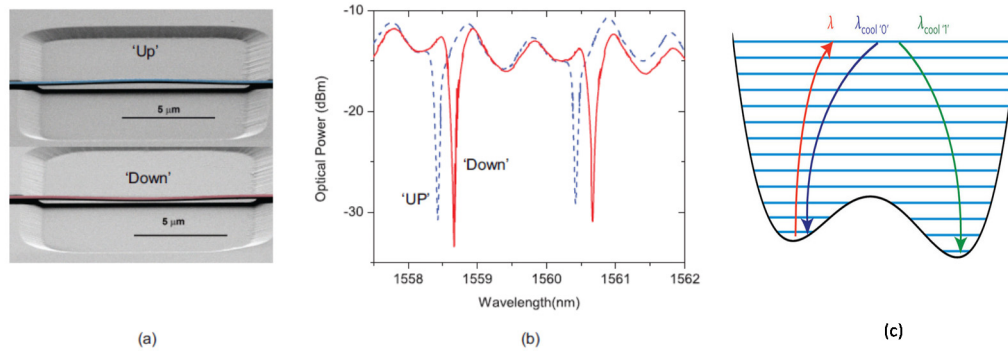


Fig. 9. Buckled NEMS amplifier for demonstrating high amplitude NEMS.

In our experiments, in order to actively manipulate the mechanical resonator via retarded optical force, the mechanical resonators are embedded in an optical race-track cavity coupled to a bus waveguide. The two mechanical states are discriminated in optical transmission measurements because the optical mode has different effective refractive indices in the two states: when the waveguide is closer to the substrate (buckled-down state) the effective refractive index is larger than in the buckled-up state. When the nanomechanical resonator resides in the buckled-down state, optical drive blue-detuned from the optical cavity resonance will initiate an optomechanical amplification process and start coherent oscillations of the nanomechanical resonator. If the kinetic energy of the mechanical resonator becomes larger than the double-well potential barrier, the beam can relax into either of the two potential wells after the excitation has been turned off. We can deterministically select the nanomechanical final state by utilizing optical cooling offered by cavity optomechanics. Differing from amplification due to a blue-detuned laser light, a red-detuned laser light dampens the oscillations of the nanomechanical resonator. In this scheme, the amplification laser is tuned to excite coherent mechanical oscillations in the resonator, whereas the cooling laser is tuned to dampen the oscillations towards either of the two discrete mechanical states. The final state can be selected by tuning the damping laser to the red side of either of the corresponding optical resonances

2.5. Investigation of fundamental phase noise of very high Q SiN nanomechanical resonators.

High Q is highly desirable since it implies weaker link to thermal bath, higher sensitivity to external signals, and lower minimum operating power. To enable real world applications based on such devices, understanding the underlying dissipation and noise mechanism is crucial.

By using high stress SiN photonic platform we developed in the ORCHID program, we have developed optically transduced, ultra high Q nanomechanical resonators ($Q > 2$ million) which allow us to measure the resonator's frequency and phase noise at unprecedented precision. This work represents the first measurement of frequency noise in ultrahigh Q nanomechanical resonators, as well as the first theoretical attempt to understand the underlying noise processes. Our model allows us to separate the amplitude fluctuations and phase fluctuations, and further extract the resonator's intrinsic frequency noise. We found the surprising effect that high Q resonators are actually more susceptible to the resonator's frequency noise. Our measurement sheds first lights on the noise mechanisms of high Q resonators. The result suggests that defect motion with broadly distributed relaxation times is responsible for the observed frequency fluctuations in high Q nanomechanical devices. This result is important for understanding the noise mechanism of the high Q silicon nitride nanomechanical resonators, as well as for applying this high performance device to sensing and oscillator applications.

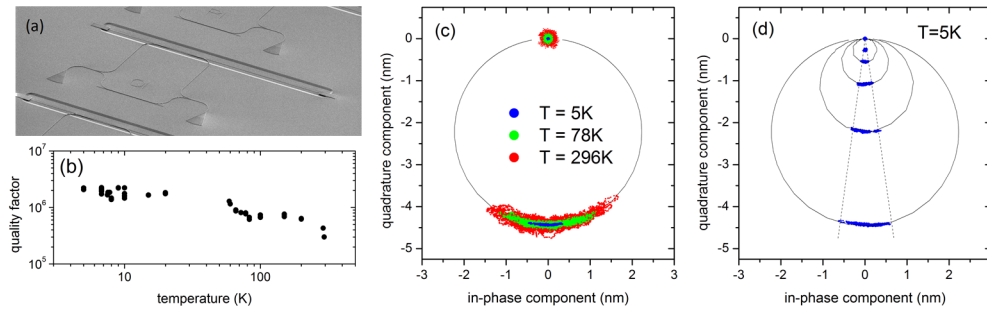


Fig. 10. $1/f$ phase noise and thermomechanical phase noise demonstration in very high Q nanomechanical resonators.

2.6. What did not work in Phase I.

We proposed detuned cavity cooling in the original proposal. As the program progressed, since there were a lot of excellent results in the orchid program working on cooling efforts, we decided to focus more on detuned amplification, which should be more interesting in terms of practical device applications. Indeed our work on detuned cavity amplification has produced many interesting results. These include (1) high amplitude NEMS and cascaded phonon generation; (2) low phase noise oscillator; (3) Regenerative optomechanical oscillators.

At phase I to phase II transition, we revisited our cooling efforts. We decided to take a different approach from what we originally proposed. Instead of using detuned cooling (essentially an

optical force effect), we combine the device with strong electromechanical coupling (adding an electrical force). In this way, in addition to the passive cavity effect, we obtained very strong parametrical electromechanical coupling that is tunable by dc-bias. Starting from room temperature with a device with mechanical Q of 160,000 we were able to first squeeze the thermal noise by more than 16dB via parametric effect. Then when we further turned on feedback cooling, our signal-to-noise allowed us to achieve a cooling factor of 5000 down to below 100mK.

2.7. What have we learned from phase I.

1. Optomechanical interaction, despite of its unprecedented sensitivity, is inherently a weak force comparing to the electrostatic force (and piezoelectric force) from actuation point view. Strong coupling remains difficult to achieve in optomechanics even with devices having best overlap of optical and mechanical modes.
2. Strong carrier effects prevent cryogenic cooling of small mode volume devices to base temperature. 2D cavities could partially remedy the thermal effect. Devices made from wideband semiconductor are required to fully circumvent this problem.
3. Optomechanical oscillator (OMO) utilizing cavity feedback has limited phase noise performance due to the phase noise of laser and the cavity drift in response to environmental effects.
4. Z-parameter, although a good figure of merit for advancing device technology, does not truly govern the final device performances for specific applications.

3. Summary of Phase II efforts: cavity electro-optomechanics and cavity piezo-optomechanics

3.1. From cavity optomechanics to cavity electro-optomechanics

After pushing the device limits in Phase I on cavity Optomechanics, our phase II efforts placed significant emphasis on enhancing the actuation efficiency of optomechanical oscillators. A central goal in this period was to increase mechanical resonant frequency by applying electric force to drive the resonator. This new cavity electro-optomechanical system combines strong electrical actuation with ultrasensitive displacement readout by optical cavity. With electro-optomechanical system, we can operate much stiffer devices (therefore much higher frequency) than devices transduced by radiation effect. Electrical actuation of the optomechanical resonators could enable feedback cooling or amplification of mechanical resonators for realizing low phase noise oscillators.

Most of our Phase II devices leverage the cavity piezo-optomechanics based on AlN-on-insulator material platform we developed in 2011. Compared with micromechanical resonators using electrostatic effects, piezoelectric transduction is particularly attractive for ultrahigh-frequency applications, such as thin-film bulk acoustic resonators and contour-mode resonators. We demonstrated that such AlN optomechanical resonators can be excited more efficiently by

piezoelectric force and we observe driven response up to 10.5 GHz. Our work points to a direction for building a class of piezooptomechanical systems with an additional electrical degree of freedom. Figure 11 illustrates our progressing chart in terms of material and device technologies.

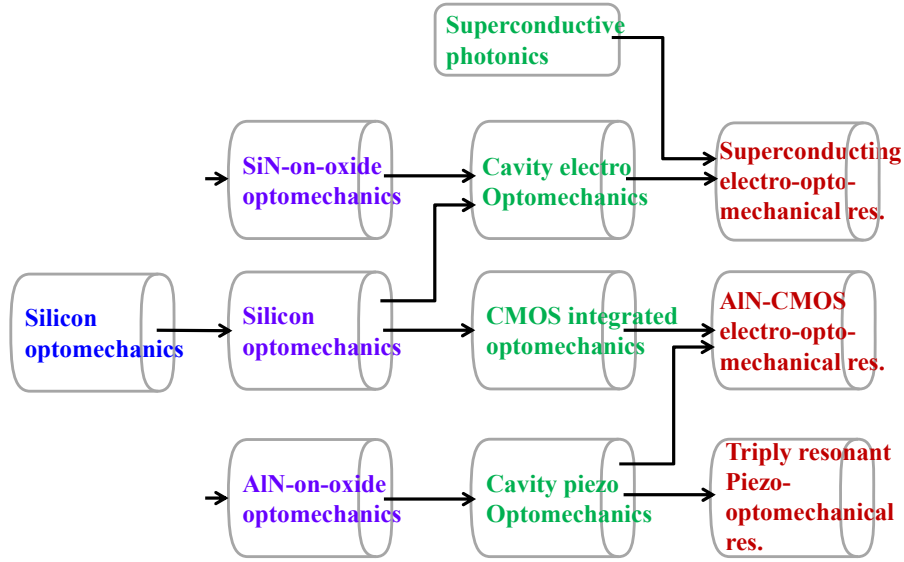


Fig. 11. Yale/Columbia team's progress flow chart on developing new materials and device platforms for Optomechanics.

3.2. Silicon cavity electro-optomechanics: advancing to SHF operation

As we mentioned earlier, an important task for building optomechanical systems is to push for higher mechanical resonant frequencies. In Phase II, our initial efforts focused on silicon electro-optomechanics system and we had successfully advanced our mechanical resonances from 1GHz to 6GHz and beyond. A range of devices have realized this program goal. In a sun-sunflower structure we published in Optics Letters (Zhang et al, 2012), we fabricated a 1.16- μm -radius disk cavity with ultrahigh quality (Q) factor by embedding the disk into a sunflower-type circular photonic crystal (CPC). The band gap of the CPC reduces the bending loss of the whispering-gallery mode of the disk, leading to a simulated Q of 10^7 , at least one order of magnitude higher than a bare disk of the same size. The design was experimentally verified with a record high loaded Q of 7.4×10^5 measured from an optimized device fabricated on a silicon-on-insulator substrate. The wavelength-sized disk radius and ultrahigh Q make such sunflower-disk cavities an ideal candidate for applications in enhanced light-matter interaction, low-threshold lasing, high-frequency nano-optomechanical transduction, and so on.

We also developed an all-integrated optoelectromechanical system that operates in the superhigh frequency band. Shown in Figure 12, this system is based on an ultrahigh- Q slotted photonic crystal (PhC) nanocavity formed by two PhC membranes, one of which is patterned with electrode and capacitively driven. The strong simultaneous electromechanical and optomechanical interactions yield efficient electrical excitation and sensitive optical transduction of the bulk

acoustic modes of the PhC membrane. These modes are identified up to a frequency of 4.20 GHz, with their mechanical Q factors ranging from 240 to 1,730. Directly linking signals in microwave and optical domains, such optoelectromechanical systems will find applications in microwave photonics in addition to those that utilize the electromechanical and optomechanical interactions separately. Such optoelectromechanical systems provide a direct link between electromagnetic signals in the optical and microwave domains and are expected to find their applications in coherent signal processing in addition to low-phase-noise optoacoustic oscillators and quantum ground-state cooling.

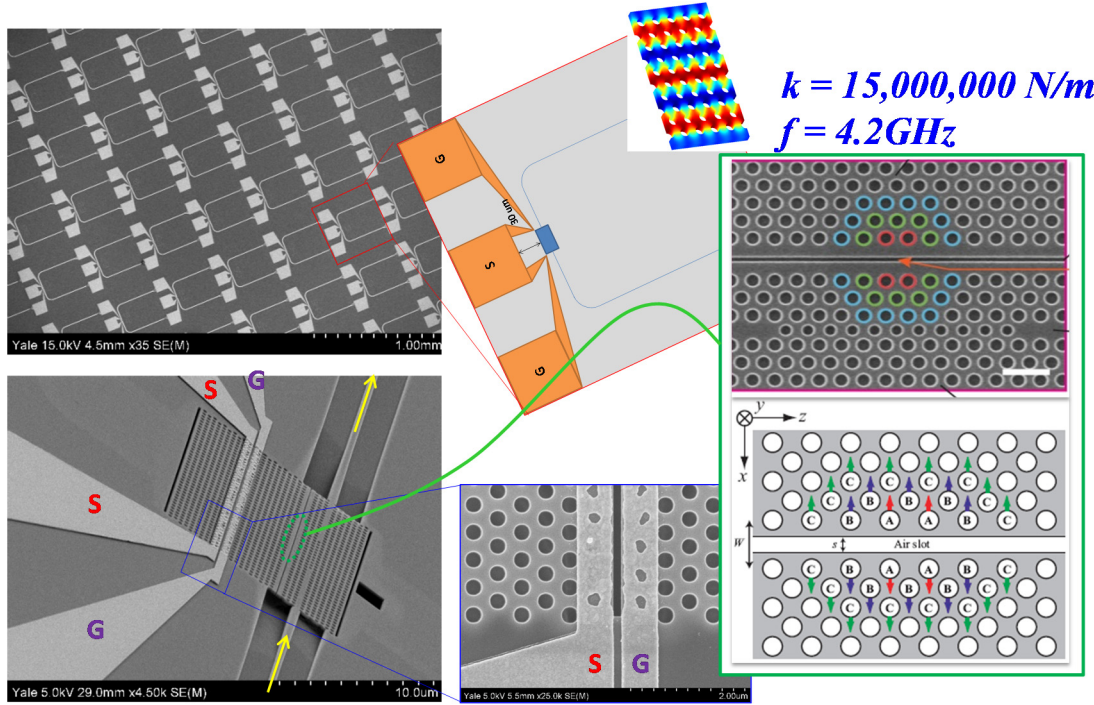


Fig. 12. Silicon electro-optomechanical cavity at super high frequencies.

3.3. SiN electro-optomechanics: 15dB thermal noise squeezing

HS SiN-on-Insulator is an earlier platform developed by Yale graduate student King Yan Fong for demonstrating optomechanics with extremely high mechanical Quality factors. In phase II, we continued to advance this material platform to allow integration of electromechanical actuation of SiN resonators.

A typical SiN electro-opto-mechanical resonator is illustrated in Fig. 13 where the device consists of SiN photonic circuits and a mechanical resonator that can be displaced by applying a voltage between two electrodes. The deflection modifies the effective refractive index of the waveguide, thereby phase-shifting the light traveling through it. By integrating the waveguide in one of the arms of a Mach-Zehnder interferometer (MZI) this phase shift is detected. Note again that our device do not rely on light within a narrow wavelength range in contrast to cavity-based systems: In principle, the operation wavelength is only limited by the bandwidth of the waveguides used (the cut-off wavelength of the waveguide is around 1800 nm), but in our current

implementation the wavelength range is set by the transmission window of the grating couplers spanning up to 50 nm in the telecom wavelength range. The mechanical part of the device shown in Fig. 15(b) consists of four SiN arms with width $w_a = 500\text{nm}$ and length $L_a = 100\text{ }\mu\text{m}$. One side of the arms is fixed at the clamping points and the other side is connected to a block at the center of the resonator, forming an “H” (Fig. 13). An electrode runs over one pair of arms and is separated from a second, fixed, electrode by a small gap. The most important point of our H-resonator design is that the electrodes are far away from the waveguide thus avoiding absorption of the light in the metal.

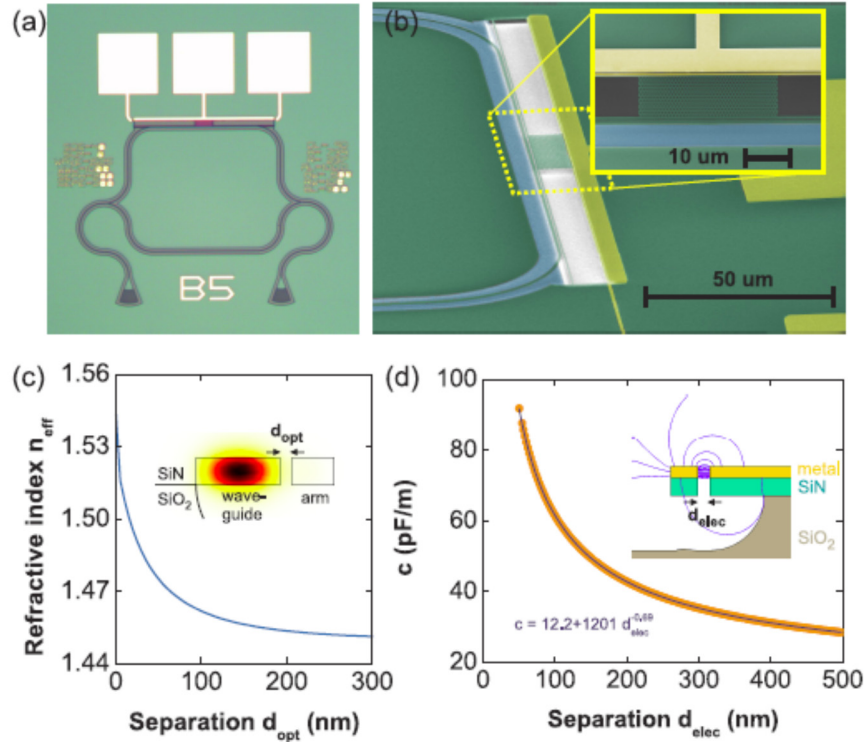


Fig. 13. Thermal noise squeezing (15dB) in SiN electro-optomechanical resonators.

The electrostatic force is 1000x times larger than optical force at typical operation conditions (Fig. 13c&d). Therefore the optical force can be safely ignored. The strong electrostatic force and the high efficiency optical transduction allow us to demonstrate parametric squeezing of the nanomechanical resonator. Using a stabilizing quadrature-feedback scheme, we show that the thermal noise can be squeezed far beyond the limit of parametric squeezing (3dB). Furthermore, by combining the feedback and parametric pumping a record of 15.1 dB of thermomechanical noise squeezing was demonstrated by the Yale group (Poot et al, NJP 2015). This not only largely exceeds the 3 dB limit for regular squeezing, but is also deeper than ever can be achieved with feedback cooling. In the same paper, the detector-resonator interaction is analyzed within the semi-classical framework and it is shown that using this feedback-stabilized parametric pumping technique true quantum-squeezed states can be prepared when the resonator starts off close to its

ground state, and that the ultimate amount of squeezing depends on the minimum detuning that can be achieved. (Fig. 14)

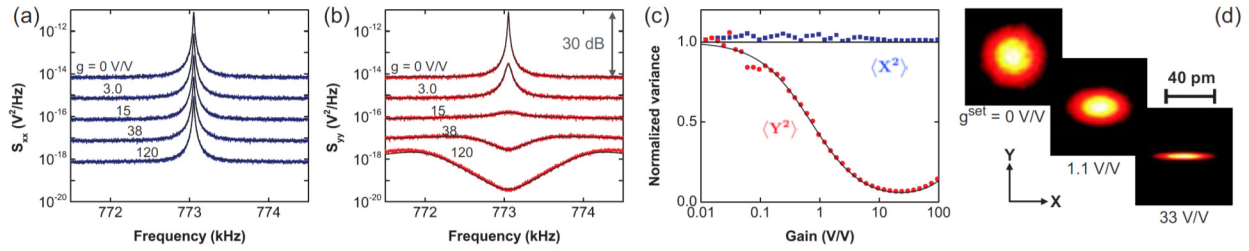


Fig. 14. Thermal noise squeezing (15dB) in SiN electro-optomechanical resonators.

3.4. AlN piezo-optomechanical system.

Silicon photonics has been regarded as a gold standard platform for integrated optomechanical circuits. However, silicon is limited to wavelengths above 1.1 μm and does not allow device operation in the visible spectrum range where low noise lasers are conveniently available. The narrow band gap of silicon also makes silicon optomechanical devices susceptible to strong two-photon absorption and free carrier absorption, which often introduce strong thermal effect that limit the devices' stability and cooling performance. In Phase I of ORCHID program, Yale graduate student Chi Xiong developed AlN-on-silicon platform for low loss, wideband optical guiding, as well as its use for achieving simultaneous high optical quality and mechanical quality optomechanical devices. Our results suggest that low cost AlN-on-silicon photonic circuits are excellent substitutes for CMOS-compatible photonic circuits for building new functional optomechanical devices that are free from carrier effects.

The AlN-on-insulator substrate has a layered structure that resemble the silicon-on-insulator wafers which are widely used in silicon photonics. 100 mm Silicon carrier wafers are thermally oxidized to provide an optical buffer layer with low refractive index (1.45 for SiO_2). The buffer layer is grown to a thickness of 2 - 2.6 μm . Subsequently AlN thin films are deposited onto the oxide. Figure 15 shows a cross sectional scanning electron micrograph of a patterned AlN waveguide sitting on 2 μm thick thermally grown SiO_2 on silicon substrates. From the obtained data we determine an average top surface roughness of 1.2 nm rms (due to the sputtering process employed) and a sidewall roughness of 3.5 nm, well below the target wavelengths used in the current study.

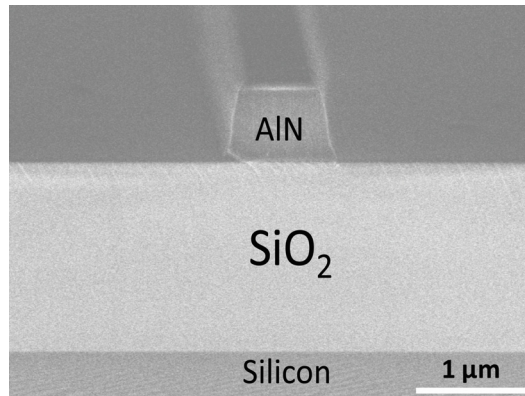


Figure 15. A cross sectional SEM image of a patterned AlN waveguide (Height: 650 nm. Width: 1 μm) sitting on 2 μm thick thermally grown SiO₂ on silicon substrates.

In this section, we show an example of AlN piezo-optomechanical resonator we designed and fabricated monolithically. Shown in Figure 16 is an integrated radial contour-mode AlN mechanical ring resonator which simultaneously serves as an optical cavity for sensitive displacement readout. We measure high optical quality factor (loaded $Q > 125,000$). The strong optomechanical interaction allows us to resolve the thermomechanical motion of the ring's contour modes with resonance frequencies in excess of GHz at room temperature and ambient pressure. The 1st contour mode ("breathing" mode) is detected at 47.3 MHz with a measured Q of 1,742 [figure 15(b)]. The 2nd contour mode ("pinch" mode) at 1.04 GHz has a slightly higher measured Q of 2,473 [figure 16 (c)]. In addition, a 30.64-MHz resonance is observed and identified as one of the wineglass modes (circumferential number $n = 4$, "square" mode [40]) with a measured Q of 1,200. By comparing the expected displacement noise with the measured RF spectral density, we can calibrate the amplitude of the Brownian motion for each mechanical mode. The displacement sensitivity corresponds to the noise floor of the spectrum. It is also noteworthy that the 1.04 GHz mode shows the best displacement sensitivity of $6.2 \times 10^{-18} \text{ m}/\sqrt{\text{Hz}}$.

Compared with conventional materials for integrated cavity optomechanical systems (such as silicon and silicon nitride), AlN offers many unique optical and mechanical properties. Its wide bandgap (6.2 eV) provides superior suppression of two-photon absorption and thus enables more stable optical resonators with high power handling capability. More importantly, AlN has a large piezoelectric coefficient, which make AlN resonators an interesting platform to implement tunable, electrically driven and optically read out oscillator systems.

The potential of AlN photonic technologies lies in the fact that wafer-scale deposition of high quality films can be conducted in a mature procedure compatible with CMOS manufacturing. The nature of the AlN sputtering process also makes it possible to design three dimensional and multi-layer structures which can enable more flexible and efficient integration. Using our fully CMOS-compatible AlN photonic circuits, we have thus implemented a promising platform for integrated optomechanical circuits with on chip signal processing capability.

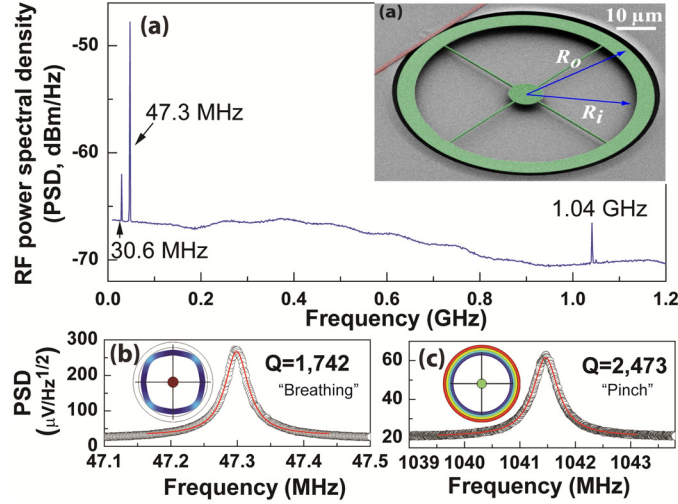


Figure 16. AlN piezo-optomechanical microwheel resonator operating from MHz to GHz ranges

3.5. Development of the first S-band AlN 1D piezo-optomechanical cavity

Along the direction of cavity piezo-optomechanics, in order to create small modal volume, high mechanical Q and high optical resonators, in Year 3 of this program we developed a piezoelectrically actuated, one-dimensional acoustic and photonic nanocavity fabricated from aluminum nitride (AlN). The device design and the simulated photonic/phononic band structure is shown in Figure 17.

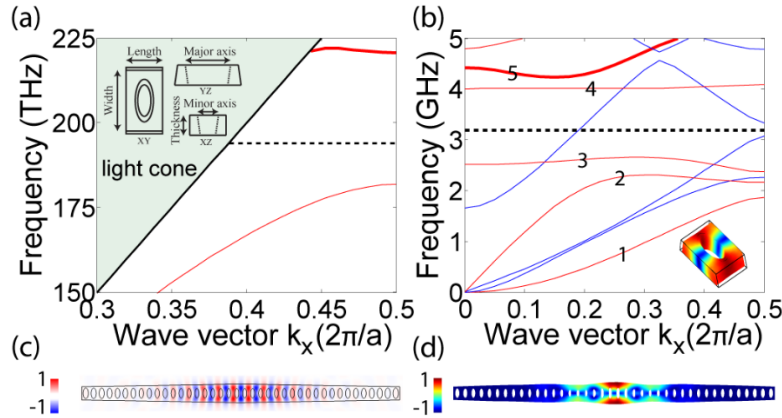


Figure 17. Design and simulation of photonic/phononic band structure of 1D AlN nanobeam resonator.

Through simultaneous band structure engineering in both photonic and acoustic domains, we obtain high-quality piezo-acousto-photonic crystal nanocavities with intrinsic optical Q of 1.2×10^5 . The piezoelectric actuation of the confined mechanical mode at 3.18 GHz is demonstrated with mechanical Q exceeding 10,000. From these measurement results we are able to calculate the magnitude of the piezoelectric force exerted on our piezo-acousto-photonic crystal nanocavity. The piezoelectric force is given by $m_{eff} \omega_r^2 x_r / Q_m \approx 54.1$ nN for 0 dBm RF power. For comparison

we estimate the electrostatic dipole force $c(V_{dc}^2 + 2V_{dc}V_{rf})$ under similar conditions, where V_{dc} and V_{rf} are the DC and RF voltages respectively, and c is the force constant of ~ 2 pN/V² for our experiment configuration. Hence, if we were to obtain the same magnitude of force as in our piezoelectric case by instead using only electrostatic actuation, the gap between the electrode and the chip's grounding plane had to be reduced from 50 to 0.3 μ m, assuming 1 V dc bias at 0 dBm RF power. Realizing such a small gap will degrade the performance of optical cavity due to the metal absorption.

Compared with electrostatic dipole forces, the piezoelectric force provides much higher actuation efficiency and is easier for utilization in experiments. The piezo-acousto-phonic crystal nanocavities can find rich applications in coherent signal processing, opto-acoustic oscillators, mechanical sensors, and beyond. Some of these applications were addressed by our follow-on papers by graduate student Kingyan Fong, Xu Han and Linran Fan.

3.6. Development of X-band piezo-optomechanical oscillator

Achieving optomechanical resonators vibrating at high frequency regime is important: from a quantum physics perspective, higher mechanical frequency translates to higher phonon energy quantum and so leads to less stringent temperature requirement for reaching mechanical ground state; from an application standpoint, high-frequency optomechanical oscillators create opportunities for high-performance microwave sources which are in demand for modern communications, networking and radio-over-fiber applications.

From very beginning of this program, we set our frequency goal as x-band mechanical resonance. Recently we were able to demonstrate devices working in this frequency regime. The main challenge is that mechanical resonators operating at high frequencies are extremely stiff, having spring constant on the order of 10^7 N/m. This high stiffness not only requires high sensitivity readout also desires high actuation efficiency – both can be realized in cavity piezo-optomechanical system.

In this section, we report a triple-resonance cavity electro-optomechanical system at X-band frequency, in which mechanical and optical modes supported in an AlN microwheel cavity are coupled to a microwave resonance supported in a half-lambda microstrip resonator. Such design combines strong piezoelectric actuation and ultrasensitive displacement readout of an optomechanical cavity which greatly improve the overall electro-optomechanical transduction. Using this triply-resonant electro-optomechanical resonators as the frequency selection component, we are able to demonstrate self-sustaining microwave oscillations at 8.256 GHz with phase noise as low as -88 dBc/Hz at 10 kHz offset from the carrier. This high-performance chip-based oscillator is expected to meet the demand for stable high frequencies sources in communications and radar system. Moreover, it provides a hybrid information-conversion system between microwave and optical domains, creating the opportunities for building integrated information networks with high complexity and efficiency.

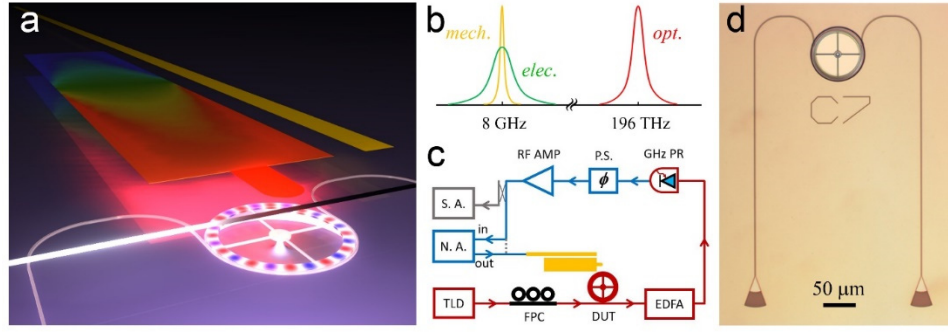


Figure 18. Triple-resonance electro-optomechanical oscillator

A schematic of the triple-resonance system is shown in Fig. 18a. The microwheel structure serves as both the high-finesse optical cavity and the high- Q mechanical resonator, which are coupled to each other through radiation pressure. Meanwhile, the microwheel's mechanical motions are piezoelectrically coupled to the microstrip resonator, whose resonant frequency is carefully designed to match that of the mechanical mode so that the actuation electric field can be resonantly enhanced. Fig. 18b illustrates the frequency scales of the three modes used in our triple-resonance system: the optical whispering-gallery-modes at around 196 THz, the high-order mechanical radial-contour mode at around 8 GHz, and the fundamental mode of the half-lambda microstrip resonator with frequency aligned to that of the mechanical mode. With the optimized optical transduction and resonantly enhanced piezoelectric actuation, our triple-resonator gives an unprecedentedly high transduction efficiency and excellent signal-to-noise ratio for super-high-frequency mechanical oscillation.

We further utilize our system to construct a low-phase noise X-band oscillator. The open-loop characterization identifies a mechanical resonance at 8.256 GHz with a Q -factor of $Q_M = 1,400$. The closed-loop oscillator is formed by feeding back the transduced signal to the microstrip resonator. Self-oscillation starts when the RF amplifiers and the EDFA provide sufficient gain to compensate the loop loss. The Barkhausen criterion for phase is fulfilled by adjusting the phase shifter. The power spectrum in the inset of Fig. 18 shows the oscillation signal at 8.256 GHz with a microwave carrier power of 6.8 dBm. The oscillator demonstrates an excellent phase noise of -88 dBc/Hz at 10 kHz offset. (Fig. 18) At large offset frequency, the phase noise reaches the noise floor of -131 dBc/Hz. A $1/f^2$ dependence is observed in the range of 10 kHz \sim 1 MHz. In the low offset frequency region (<10 kHz), the phase noise is dominated by flicker noise of the RF amplifiers which appears as the $1/f^3$ dependence in the spectrum. Further reduction of phase noise can be achieved by using amplifiers with lower flicker noise and minimizing the optical insertion loss.

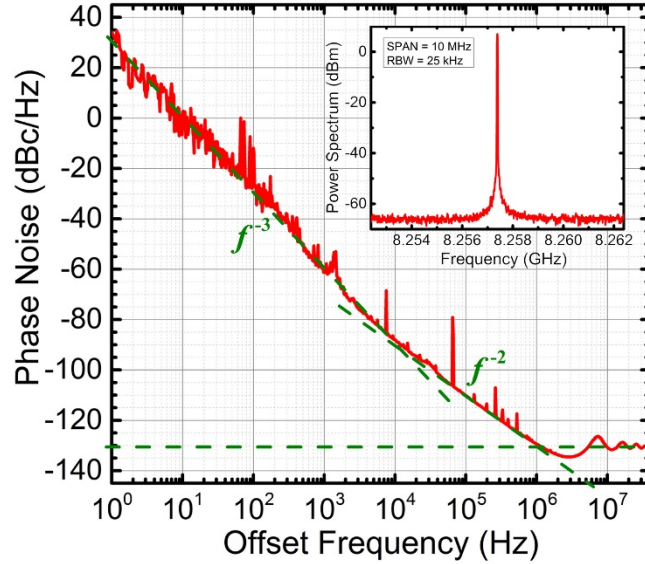


Figure 19. Phase noise Performance characterization of the 8.256 GHz oscillator.

The super high frequency mechanical resonator we show here is realized at room temperature. Operating a similar device at 300 mK in a He^3 fridge would place both mechanical and microwave modes at ground state and enable a quantum interface between microwave and optical fields when the high- Q microstrip resonator is fabricated from superconducting materials.

For future development, improving the spectral purity of an oscillator requires improving the Q -factor of resonant element as well as reducing the loss inside the feedback loop. For high frequency resonance, the Q -factor of the mechanical mode is limited by the fQ product. In our case, the X-band mechanical mode has an fQ product of 1.15×10^{13} which is close to the limit of AlN reported in literature by Tom Kenny's group. The major loss in the loop comes from the intrinsic loss in the electrical-to-optical transduction. This loss deteriorates the signal to noise ratio and sets lower limit of the necessary amplification, hence determining the noise floor of the oscillator signal. This transduction loss can in principle be improved by increasing the optical pump power. It is also possible to improve the photon detection efficiency by integrating on-chip photoreceivers, with which an on-chip high frequency microwave source with even better phase noise performance can be expected.

3.7. A 10.5GHz piezo-optomechanical oscillator

One can increase the mechanical frequency further by utilizing higher order radial counter modes. However, we found signal reduction for higher order modes. This is understandable because our drive utilizes a single electrode which does not favor the excitation of higher modes. Also, the optomechanical coupling efficiency drops when the acoustic oscillates too rapidly along the perimeter of the microresonator. For a long period of time, we had thought that we were hitting a hard limit below 10GHz.

Fortunately, there are another group of modes which scale better at high frequencies. In a recent APL paper [Xu et al 2014], we report on the advance of chip-scale cavity optomechanical resonators to beyond 10 GHz by exploiting the acoustic thickness mode of an aluminum nitride micro-disk. By engineering the mechanical anchor to minimize the acoustic loss, a quality factor of 1 830 and hence a frequency-quality factor product of 1.9×10^{13} Hz are achieved in ambient air at room temperature. Actuated by strong piezo-electric force, the micro-disk resonator shows an excellent electro-optomechanical transduction efficiency. Our detailed analysis of the electro-optomechanical coupling allows identification and full quantification of various acoustic modes spanning from super-high to X-band microwave frequencies measured in the thin film resonator.

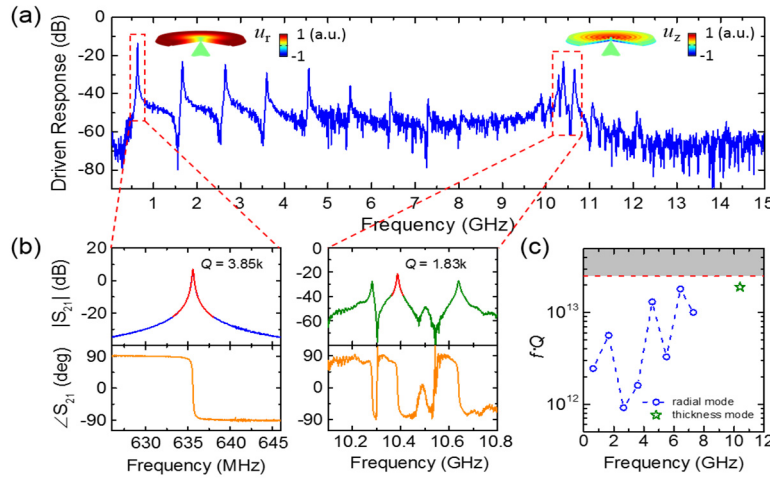


Figure 20. Optomechanical oscillator operating at 10.5GHz

Figure 20(a) shows a broad-band driven response spectrum of the disk with radius $5.5 \mu\text{m}$ at a blue cavity detuning around 1553.5 nm. Mechanical resonance peaks up to above 10 GHz are clearly resolved. The fundamental radial-contour mode is observed at 636 MHz as the first resonance peak, which matches well with the simulated value of 632 MHz using COMSOL. Starting from the second peak at 1.67 GHz, higher-order radial-contour modes can be distinctly identified up to the 9th-order at 8.06 GHz. It can be seen that, as the mode order and frequency increase, the resonance signal of the radial-contour mode gradually decreases and finally becomes indistinguishable from the background noise. Surprisingly, the resonance peak at 10.4 GHz remarkably stands out, indicating its different origin from the high-order radial-contour modes. Zoomed-in spectra of fundamental radial breathing and thickness modes are shown in Fig. 20(b). A phase shift of 180 degree is observed at each resonance. The Q factors measured in air are fitted to be 3 850 and 1 830, respectively. Such high Q factors can be attributed to the carefully minimized anchor contact which significantly reduces the anchor loss. The fQ products of the first eight radial-contour modes as well as the fundamental thickness mode are plotted in Fig. 20(c). Although the fQ products of radial-contour modes have a trend to increase with frequency, the fast decay of the transmission signal of high order contour modes inevitably limits their practical

applications. On the other hand, the thickness mode exhibits both excellent transmission and a highest fQ product of 1.9×10^{13} Hz, which is close to the theoretical limit of 2.5×10^{13} Hz.

Looking forward, it is possible to operate the mechanical resonator at even higher frequency for example at harmonics of the thickness modes, 20.8GHz and 31.2GHz, since we already showed that the thickness mode can be easily scaled to high frequency regime while maintaining good optical confinement. The thickness mode-based piezo-optomechanical resonator could also be used as mechanical transducer in a hybrid platform for efficient information processing and conversion among different domains.

3.8. Packaging of optomechanical oscillator

Low phase noise oscillators demand robust electrical and optical interfaces. In Phase II, we designed two packaging solutions, respectively for 3GHz and 10GHz oscillators. Shown in Figure 20a is a complete 3GHz package which uses an input grating coupler to take external light from a fiber pigtailed laser and an output grating coupler to send the transmitted light to a near field photodetector. In this package, we installed 4 input fibers. Only two are used – one for laser input, one for calibration port output during alignment. The detector and TIA were assembled on a regular circuitboard which was flip-aligned with the resonator chip.

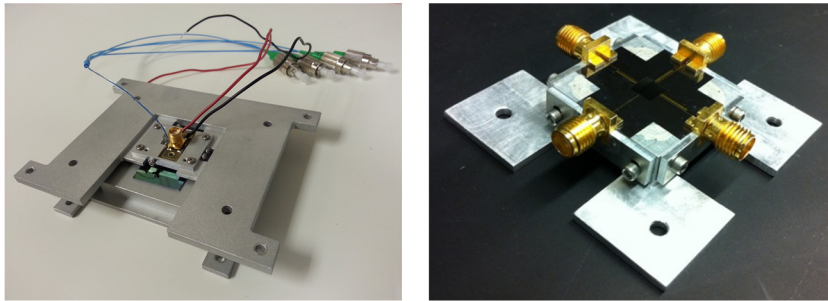


Figure 21. Assembled electro-opto-mechanical oscillators for 3GHz and 10GHz operations.

The 10GHz package uses a sapphire substrate to build the electrical resonator. The sapphire is only 125um thick so that light can transmit through the sapphire onto the resonator chip without experiencing optical loss. The thin sapphire also allows us to make compact electrical resonators for interfacing with the AlN resonators. In the package shown in Fig. 20b, we incorporated four electrical resonators of different sizes to match mechanical resonators operating at different frequencies.

3.9. Parametric optomechanical oscillations in 2D slot-type high-Q PhC cavities and feedback and harmonic locking for low-noise reference clocks

Subsequently we experimentally demonstrate the optomechanical cavity based on the air-slot PhC cavity [Fig.22(a)] with optical quality factor $Q_o = 4.2 \times 10^4$ and a small modal volume of 0.05 cubic wavelengths [Fig.22(b)-(c)]. The optical mode is coupled with the in-plane mechanical modes with frequencies up to hundreds of MHz. The fundamental mechanical mode shows a frequency of 65 MHz and a mechanical quality factor of 376 [Fig.22(d)]. The optical spring effect,

optical damping, and amplification are observed [Fig.22(e)-(f)] with a large experimental optomechanical coupling rate $g_{om}/2\pi$ of 154 GHz/nm, corresponding to a vacuum optomechanical coupling rate $g^*/2\pi$ of 707 kHz. With sub-mW or less input power levels, the cavity exhibits strong parametric oscillations. The phase noise of the photonic crystal optomechanical oscillator is also measured.

To reduce the long-term phase noise, feedback and harmonic locking techniques to external low-noise reference clocks are experimentally performed, with suppressed timing jitter by three orders of magnitude. The feedback and compensation techniques significantly reduce the close-to-carrier phase noise, especially within the locking bandwidth for the integral root-mean-square timing jitter [Fig.22(j)]. Harmonic locking via high-order carrier signals is also demonstrated with similar phase noise and integrated root-mean-square timing jitter reduction [Fig.2(h)-(j)]. The chip-scale optomechanical oscillators are tunable over an 80-kHz range by tracking the reference clock, with potential applications in tunable radiofrequency photonics platforms.

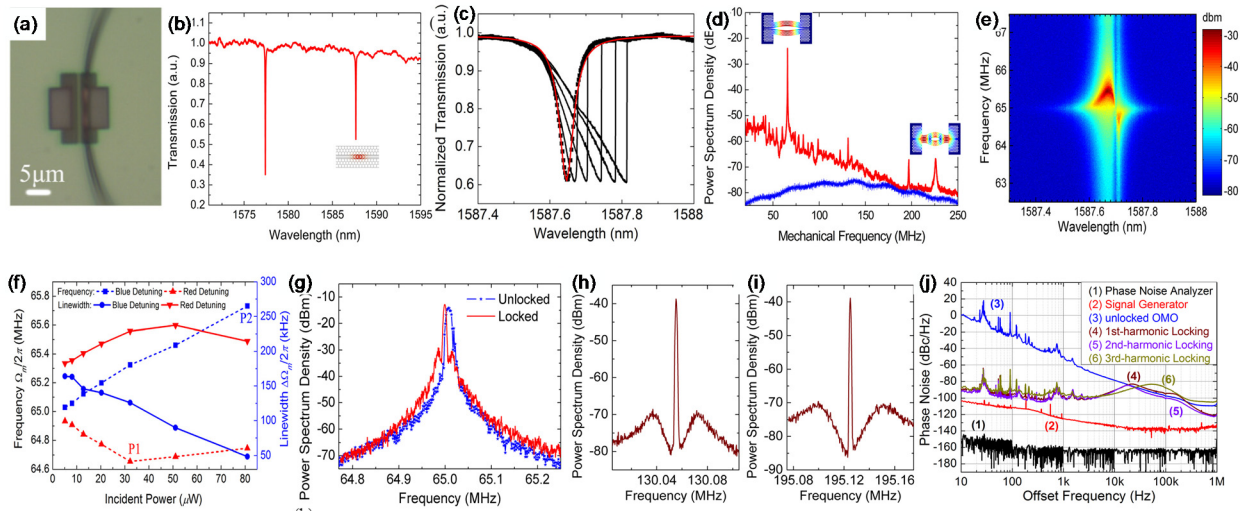


Fig. 22. Parametric optomechanical oscillations in two-dimensional slot-type high-Q PhC cavities and feedback and harmonic locking for low-noise oscillators.

3.10. CMOS monolithically integrated optomechanical resonators

Another important milestone of our ORCHID program is the first demonstration of a cavity optoelectromechanical system integrated monolithically with high-efficiency germanium detector on a CMOS-compatible platform. Monolithically integrated micro- and nanoelectromechanical systems were realized long time ago but they suffer from limited operational bandwidth and relatively low transduction efficiency. Optomechanics offers high bandwidth and very high transduction efficiency, however, the loss associated with fiber-to-chip coupling poses a practical obstacle to many applications that require high-efficiency signal conversion. It is thus desirable to

have a photodetector that is monolithically integrated with the nanooptomechanical system to convert the optical signal directly to the electrical domain.

In the work by Sun et al (Optics Letter 2014), we reported the first demonstration of such a monolithically integrated cavity nanooptoelectromechanical system which takes signals from an optical input channel and delivers processed signals to an electrical output channel. The core element is a high-quality-factor optomechanical ring resonator where its in-plane mechanical modes are simultaneously coupled to an itinerant microwave and resonant optical field. Taking advantage of the high responsivity of the integrated germanium detector on the chip, the device allows for high-efficiency signal transduction of mechanical modes. The devices were fabricated at a commercial foundry and postprocessed with an additional step of photolithography and wet etching to release the optomechanical ring from the substrate. A complete device is shown in Fig. 23 which includes a high-quality-factor optomechanical ring resonator with the adjacent electrical actuation element and an integrated germanium photodetector. Under a reverse bias of 1.0 V, the photodetectors are found to possess a high responsivity of 0.51 A/W with a low dark current of 100 nA. The responsivity can be further enhanced with a larger reverse bias voltage at the expense of a larger dark current. The optomechanical ring resonator is actuated by mechanical connection to a nanobeam. The nanobeam is electromechanically driven with an ac voltage applied to the adjacent anchors which are highly doped silicon layers wired to the metal pads. The mechanical vibration signal from the electromechanical actuation is transduced into the optical domain by the optomechanical ring resonator, which is then converted back to the electrical domain by the integrated germanium photodetector.

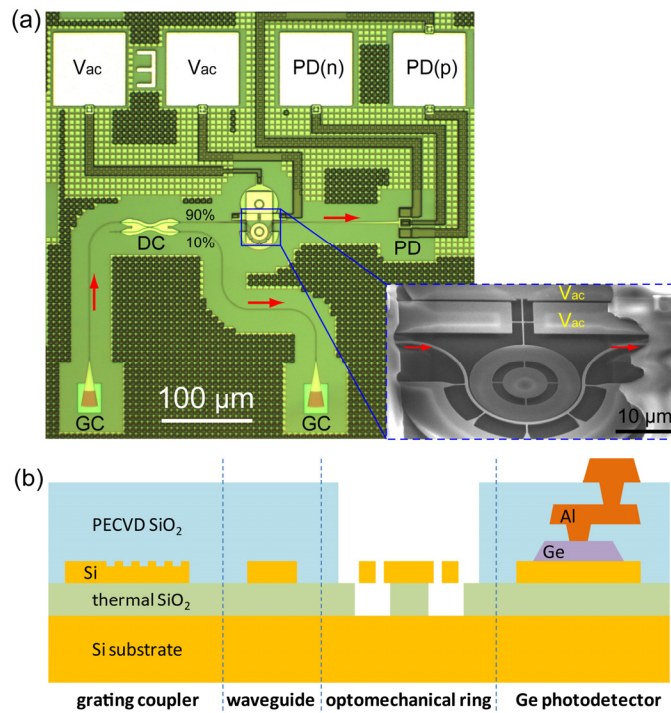


Figure 23. Monolithically integrated optomechanical oscillator on a CMOS chip with on-chip germanium detectors.

The planar geometry of the optomechanical resonator determines that all the identified mechanical resonances are actually from the in-plane mechanical motion of the ring structure. There are two types of motions categorized based on their angular symmetry: one is radial-contour modes and the other is wine-glass modes. We have identified the first 2 radial-contour modes and the first 6 wine-glass modes up to a frequency of 2.003 GHz. The theoretical frequency values are in excellent agreement with the measured ones, with a relative error within 3.3%. Overall, the wine-glass modes have relatively higher quality factors than the radial-contour modes due to their different symmetry. Operating in the UHF band, the demonstrated device could be used as optoelectronic oscillators in closed-loop configuration discussed in the previous section.

3.11. Phase noise measurement of monolithic OMO

As the key part of our Phase II program, we also demonstrated the monolithic integration of photonic crystal optomechanical oscillators and on-chip high speed Ge detectors based on the silicon CMOS platform. With the generation of both high harmonics (up to 59th order) and subharmonics (down to 1/4), our chipset provides multiple frequency tones for applications in both frequency multipliers and dividers. The phase noise is measured down to 2125 dBc/Hz at 10 kHz offset at $\sim 400 \mu\text{W}$ dropped-in powers, one of the lowest noise optomechanical oscillators to date and in room-temperature and atmospheric non-vacuum operating conditions. These characteristics enable optomechanical oscillators as a frequency reference platform for radio-frequency-photonic information processing.

Fig. 24(a) shows the designed layout of fully integrated optomechanical cavity oscillator with on-chip Ge detector, with the tapered optical Si waveguide (WG) path denoted in light blue. Laser is first coupled from free-space lenses into a low-loss inverse oxide coupler at the chip facet [Fig. 3(b)], propagating then from the oxide coupler into a silicon waveguide. The transmitted light is split equally into two paths: one into the integrated Ge detector and the other coupled out from the inverse oxide coupler to off-chip lenses for external test diagnostics. The proposed OMO is a slot-type PhC cavity consisting of two air-bridged PhC slabs separated by a narrow 120 nm air slot as shown in Fig. 3(c) and 3(d). Fig. 3(e) shows the integrated Ge detector which analyzed systematically in our previous works.

The DC I-V diode characterization and frequency response of the Ge detector are characterized firstly with the setup shown in Fig. 24(f). As shown in Fig. 24(f), the measured dark current is 500 nA at -1 V bias while a dark current of 1 μA is the typical upper bound for high-bandwidth detectors. The measured 3-dB bandwidth of the detector is 9 GHz at 0 V bias and 18.5 GHz at -1 V bias as shown in Fig. 24(g). The oscillator-integrated detector responsivity is measured as 0.58 A/W at 0 V and 0.62 A/W near -0.5 V under 1550 nm illumination of 200 μW . Fig. 24(h) illustrates the measured optical transmission spectra of the slot cavity resonances. The modeled $|E|^2$ field distributions of the resonance is shown in Fig. 3(h) inset, with intrinsic quality factor of $\sim 800,000$ for the fundamental mode. Figs. 24(i) and 24(j) show the measured RF spectra of the integrated optomechanical oscillator at blue detuning and below/above the threshold power, respectively. For a dropped-in power about -15 dBm, the measured RF spectra for both detectors in room

temperature and atmosphere show the fundamental mechanical resonance at 110.3 MHz and a cold cavity mechanical quality factor of about 480. The modeled modal resonance displacement field is shown in the inset of Fig. 24(i). By comparing results from external detector and integrated detector, our integrated Ge detector has low background noise floor that can go down to approximately -98 dBm [Fig. 24(i)]. When driven ($\sim 400 \mu\text{W}$) above threshold ($\sim 127 \mu\text{W}$), the intrinsic mechanical energy dissipation is overcome and the optomechanical resonator becomes a self-sustained OMO with narrow linewidths ($\sim 11 \text{ Hz}$), as illustrated in Fig. 3(j). The vacuum optomechanical coupling rate is determined as $\sim 0.8 \text{ MHz}$ which is much larger than other non-PhC optomechanical cavities, important to reduce the OMO threshold and improve the SNR. With higher input power of 3.2 mW, we can get the high-order harmonics from our monolithic OMO-detector chipset, due to the nonlinear optomechanical transduction from the optical lineshape. We observed RF harmonics up to 6.9 GHz [Fig. 24(k)], the 59th harmonic in this device case, which is bounded by the spectrum analyzer measurement range. Such high-harmonics can serve as high frequency reference.

Fig. 24(l) shows the single-sideband phase noise spectra of our free-running OMO chipset, for a 112.7 MHz carrier. In room temperature and atmospheric non-vacuum, our integrated OMO chipset exhibits a phase noise of approximately -103 dBc/Hz at 1 kHz offset and -125 dBc/Hz at 10 kHz offset, one of the lowest noise to date in reported OMOs. We note that at higher frequency offsets (such as 1 MHz or more), the noise floor is limited only by our detector currently as the phase noise measured simultaneously by external detector can get as low as -165 dBc/Hz at 10 MHz offset. As we can see, for offsets close-to-carrier frequency, our free running OMO has significant amount of $1/f^3$ whereas for offsets far-from-carrier frequency ($f > 100 \text{ kHz}$). Fig. 24(m) shows the Allan deviations calculated from raw phase noise and power-law fitted phase noise for the free-running OMO, and an open-loop frequency instability at 10^{-8} is observed. The consistency between different methods can be seen in Fig. 24(m) where there is small phase noise discrepancy at the close-to-carrier and far-from-carrier offsets. As shown in Fig. 24(n), the timing jitter of the oscillator is calculated from the measured phase noise integrating from 100 Hz to the carrier frequency, and should be 3.42 ps for the integrated detector and 10.01 ps for the external photodetector, with performance close to commercial electronic frequency standards.

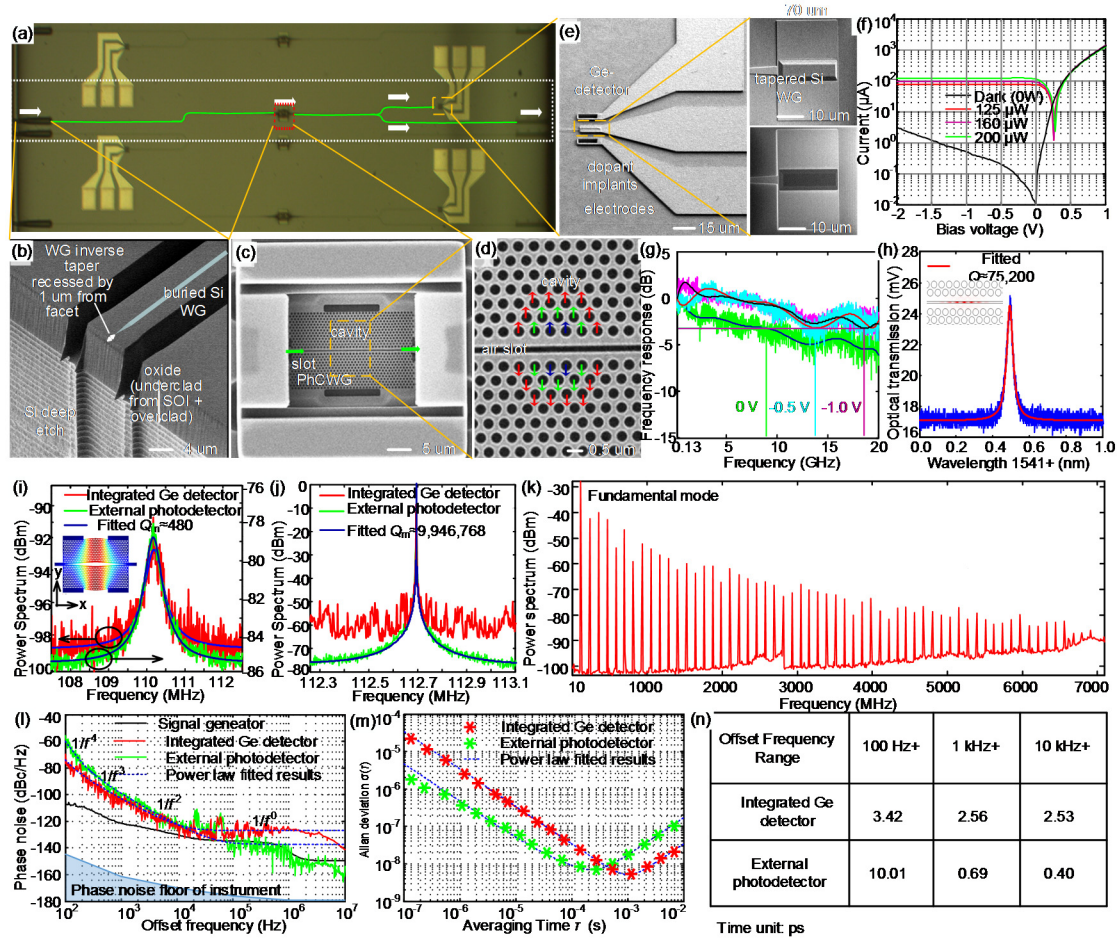


Fig. 24. A monolithic optomechanical oscillator with integrated Ge detectors.

4. Other accomplishments of fundamental interests

4.1. Photonic Bus Synchronization of Remote Nanomechanical Oscillators

Synchronization between coupled oscillatory systems is a frequent natural phenomenon and is becoming an important concept in modern physics and technology. Exploiting synchronous oscillation of coupled resonators promises to improve the performance of micro and nano-devices when power handling and high phase coherence are of critical concerns. Here we demonstrate synchronization of two nanomechanical oscillators in a single photonic ring cavity. Optical backaction gives rise to both reactive and dissipative coupling of distant mechanical resonators, leading to coherent oscillation and mutual locking of resonators with phase dynamics beyond the widely used Kuramoto model.

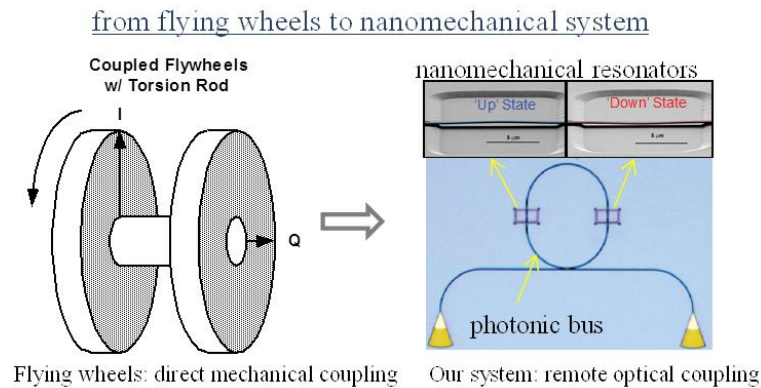


Figure 25. Coupled oscillators – from flying wheels to remotely coupled nanomechanical resonators.

Figure 25 shows our prototype device for implementing the 2-resonator coupling scheme. The device is patterned from a silicon-on-insulator wafer, with a process that has been established in our laboratory. The mechanical resonators are formed by releasing a short length of the racetrack waveguide. They are designed to have same dimensions ($10\mu\text{m}\times 500\text{nm}\times 110\text{nm}$) so that their flexural vibration modes have closely-matched resonant frequencies. The large separation between two nanomechanical resonators (more than $100\mu\text{m}$) ensures that the resonators are mechanically isolated and that any coupling between them is through the optical field.

We demonstrate a fully integrated optomechanical chip that consists of two nanomechanical oscillators linked by an optical cavity. We use cavity backaction to provide tunable coupling among the oscillators, and coerce the motion of multiple mechanically isolated oscillators into the synchronized state. The gain of the individual oscillators is acquired from the optical field which in principle only adds quantum noise. Consequently, our platform should be more stable and more scalable for building large scale arrays. Our optical interconnect topology also inherently enables all-to-all coupling, where any oscillator can be coupled to any other, which is a requisite for global synchronization among networks of distant oscillators. This platform can therefore also serve as a test bed for confirming theoretical findings by providing fully configurable on-chip resonator networks. Our studies in two-oscillator synchronization will pave the road for realizing massive synchronization of large number of oscillators.

We believe this work represents a significant advance in the basic physics of complex coupled dynamic systems. Very interestingly we found that the optical backaction induces both displacement and velocity coupling. This is a crucial difference from the simple phase-difference coupling described by the widely used Kuramoto model, and hence a plethora of new phenomena can be expected. Indeed, in our experimental platform, we show coherent oscillations and the mutual locking of resonators with phase dynamics beyond the Kuramoto model. Our theoretical analysis has found that synchronization takes place in a 3-dimensional phase space rather than the simple 1-D phase oscillations described by the standard Kuramoto model.

4.2 Dynamic dissipative cooling of strong-coupled mechanical oscillator and coupled cavities

On another hand, dynamic dissipative cooling in single cavity and motional ground-state cooling in coupled cavities were observed theoretically with red detuning. Cooling of mesoscopic mechanical resonators represents a primary concern in cavity optomechanics. In the strong optomechanical coupling regime, we proposed to dynamically control the cavity dissipation, which is able to significantly accelerate the cooling process while strongly suppressing the heating noise. Furthermore, the dynamic control is capable of overcoming quantum backaction and reducing the cooling limit by several orders of magnitude. The dynamic dissipation control provides new insights for tailoring the optomechanical interaction and offers the prospect of exploring mesoscopic quantum physics.

Moreover, motional ground-state cooling and quantum-coherent manipulation of mesoscopic mechanical systems are crucial goals in both fundamental physics and applied science. Here we demonstrated that the motional ground state can be achieved in the highly unresolved sideband regime, through coherent auxiliary cavity interferences. We further illustrated coherent strong Rabi coupling between indirectly coupled and individually optimized mechanical resonators and optical cavities through effective dark-mode interaction. The proposed approach provides a platform for quantum manipulation of mesoscopic mechanical devices beyond the resolved sideband limit.

4.3. “Phonon” radiation pressure force and cascaded optomechanical transparency

Electromagnetically induced transparency (EIT) has great theoretical and experimental importance in many physics subjects, such as atomic physics, quantum optics, and more recent cavity optomechanics. Optical delay is the most prominent feature of EIT and in cavity optomechanics optical delay is limited by mechanical dissipation rate of sideband-resolved mechanical modes. In Year 4 of the ORCHID program we demonstrated a cascaded optical transparency scheme by leveraging the parametric phonon-phonon coupling in a multimode optomechanical system, where a low damping mechanical mode in the unresolved-sideband regime is made to couple to an intermediate, high frequency mechanical mode in the resolved-sideband regime of an optical cavity. This cascaded optomechanical system fully exploits the long optical delay offered by the low damping mechanical mode without the sideband-resolved requirement, and provides enhanced functionalities and reduced system decay rate, which is critical for information processing. Extended optical delay and higher transmission, as well as optical advancing are demonstrated. These results provide a route to realize ultra-long optical delay, indicating a significant step toward integrated classical and quantum information storage devices.

Our approach leverages a new radiation-like phonon-phonon coupling mechanism that is largely overlooked in nanomechanics. In the past, the phonon-phonon coupling is often considered as higher order effect (Duffing effect) due to the mirror symmetry in standard beam resonators. However, this picture breaks down in most advanced optomechanical system, including microdisk, micro-toroid, and microwheel in this work. With engineered mechanical modes, the phonon-

phonon coupling strength can be comparable with typical superconducting electromechanical systems, thus provides a new promising route to manipulate nanomechanical resonators which is crucial in both information applications and quantum experiments.

We start with a regular optomechanical system in the resolved-sideband regime, where an optical cavity (frequency ω_o , linewidth κ) is coupled to a high frequency mechanical mode (frequency Ω_H , linewidth Γ_H) with coupling rate g_{om} . We introduce another sideband-unresolved low frequency mechanical mode (frequency Ω_L , linewidth Γ_L) which couples to the high frequency mechanical mode through parametric phonon-phonon coupling with coupling rate g_{mm} . The interaction Hamiltonian of the parametric phonon-phonon coupling has a similar form as radiation pressure coupling in optomechanical systems. In cavity optomechanical systems, the photon-phonon coupling can be strongly enhanced by a coherent optical pump, leading to EIT phenomena. Analogously the subsystem consisting of the two parametrically coupled mechanical modes should also exhibit EIT phenomena. If a weak optical probe is swept across the optical cavity, many pathway exist for the optical probe in the cavity: i) directly transmitting through the optical cavity, ii) interfering with the optical pump scattered by the high frequency mechanical mode, iii) interfering with the optical pump scattered by the phonons scattered from the mechanical pump by the low frequency mechanical mode. Beside the transparency window produced due to the high frequency mechanical mode, feature of the low frequency mechanical mode is also imprinted in the optical probe through the parametric phonon-phonon coupling with the high frequency mechanical mode serving as a bridge. The parametric phonon-phonon coupling is a key part in the cascaded EIT, which we implement in a micro-wheel structure (Fig.26). A displacement of one mechanical mode leads to tension and boundary change in the structure, thus modifying the resonant frequencies of other mechanical modes.

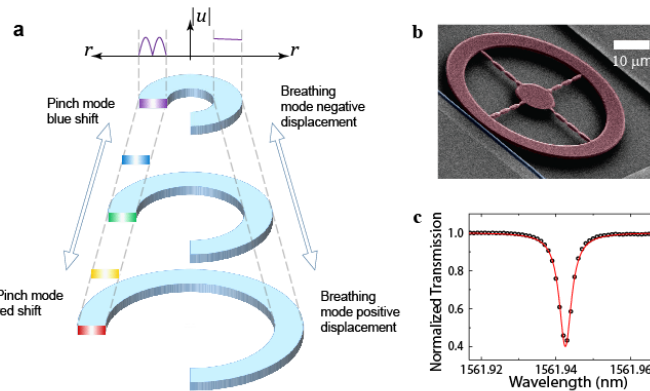


Figure 26. “Photon radiation pressure” effect and AlN microwheel device for demonstrating cascaded EIT.

By combining the parametric phonon-phonon coupling and optomechanical coupling, the cascaded EIT effect can be observed. When the optical probe is swept across the optical cavity

over a wide range, we first see the normal EIT which has a transparency window with a linewidth equal to the dissipation rate of the high frequency mechanical mode. Upon zooming into the transparency window, a second transparency window sitting on top of the original transparency window can be observed. In this case, the linewidth of the narrow transparency window equals to the dissipation rate of the low frequency mechanical mode instead of the much larger linewidth of the high frequency mode. The high frequency mechanical mode essentially mediates the coupling between the optical cavity and the low frequency mechanical mode which is in the optomechanical unresolved-sideband regime and therefore cannot be used for regular EIT. The narrow optical transparency window leads to strong optical phase modulations as shown and therefore large optical group delays, which in our case reach $5.0 \mu\text{s}$. This corresponds to a more than 8 times improvement compared with $0.6 \mu\text{s}$ delay of the regular EIT which only involves the high frequency mode. Moreover, the optical transmission is increased, and this leads to a 10 times improvement in the bandwidth-delay product

For optomechanical applications in information processing, one major obstacle is the decoherence, where the phonon lifetime plays a critical role. In our optomechanical system, the phonon lifetime for the high frequency mechanical mode is around $30 \mu\text{s}$. The phonon lifetime can be greatly increased in the cascaded multimode coupling scheme. In this scheme, the low frequency mechanical mode in the optomechanical unresolved-sideband regime functions as if it is in the optomechanical resolved-sideband regime, and the frequency just needs to exceed the linewidth of the high frequency mechanical mode. For a mechanical resonator with frequency around 200 kHz, a linewidth as low as 0.1 Hz can be realized, corresponding to a 10 s phonon lifetime. Also a higher mechanical Q can be expected for a lower frequency mechanical mode due to the empirical $f \cdot Q$ limit. Therefore the quantum coherence time, which is usually limited by the rethermalization time of the sideband-resolved mechanical mode $\tau = \hbar Q/kT$, will also be extended because of its hybridization with the high Q mechanical mode in the unresolved-sideband regime under a strong mechanical pump. Moreover, the low frequency mechanical mode can preserve the quantum state much longer due to its long rethermalization time, thus serving as a better quantum register. In essence, our cascaded coupling scheme provides a viable route to long optical delay and long coherence time by leveraging the parametric phonon-phonon coupling, pushing forward the frontier of optomechanical devices in both classical and quantum regime.

Appendix

Appendix 1. Yale/Columbia team publication list (as of 07/06/2015)

1. “Nano-optomechanical resonators in microfluidics”, K. Y. Fong, M. Poot, H. X. Tang, **Nano Letters**, submitted.
2. “A 10-GHz film-thickness-mode cavity optomechanical resonator”, X. Han, K. Y. Fong, H. X. Tang, **Applied Physics Letters**, 106, 161108 (2015)
3. “Deep feedback-stabilized parametric squeezing in an opto-electromechanical system”, M. Poot, K. Y. Fong, H. X. Tang, **New J. Physics**, 17, 043056 (2015)
4. “Cascaded optical transparency in multimode-cavity optomechanical systems”, L. R. Fan, K. Y. Fong, M. Poot, H. X. Tang, **Nature Communications** 6, 5850 (2015)
5. “Coupled cavities for motional ground-state cooling and strong optomechanical coupling”, Y.C. Liu, Y.F. Xiao, X.S. Luan, Q.H. Gong and C. W. Wong, **Phys. Rev. A** 91, 033818.
6. “Classical non-Gaussian state preparation through squeezing in an optoelectromechanical resonator”, M. Poot, H. X. Tang, **Phys. Rev. A** 90, 063809 (2014)
7. “Microwave assisted optical amplification and coherent absorption in cavity piezo-optomechanical system”, K. Y. Fong, L. R. Fan, L. Jiang, H. X. Tang, **Physical Review A** 90, 051801R, 2014
8. “An integrated low phase noise radiation-pressure-driven optomechanical oscillator chipset”, X. Luan, Y. Huang, Y. Li, J. F. McMillan, J. Zheng, S.-W. Huang, P.-C. Hsieh, T. Gu, D. Wang, A. Hati, D. A. Howe, G. Wen, M. Yu, G. Lo, D.-L. Kwong, and C. W. Wong, **Scientific Reports** 4, 6842 (2014);
9. “Phase noise of self-sustained optomechanical oscillators”, K. Y. Fong, M. Poot, X. Han, H. X. Tang, **Physical Review A** 90, 023825 (2014)
10. “The prospect of detecting single-photon force effects in cavity optomechanics”, H. X. Tang, and D. Vitali, **Physical Review A** 89, 063821 (2014)
11. “Triply resonant cavity piezo-optomechanics at X-band”, X. Han, C. Xiong, K. Y. Fong, X. F. Zhang, H. X. Tang, **New Journal of Physics** 16, 063060 (2014).
12. “Monolithically integrated, ultrahigh-frequency cavity nanooptoelectromechanical system with on-chip germanium waveguide photodetector”, X. K. Sun, K. Xu, H. X. Tang, **Optics Letters** 39, 2514 (2014)
13. “Broadband nanoelectromechanical phase shifting of light on a chip”, M. Poot, H. X. Tang, **Applied Physics Letters** 104, 061101 (2014)
14. “Photonic cavity synchronization of nanomechanical oscillators”, M. Bagheri, M. Poot, L.R. Fan, F. Marquardt, H. X. Tang, **Physical Review Letters** 111, 213902 (2013)
15. “Dynamic dissipative cooling of a mechanical oscillator in strong-coupling optomechanics”, Y.-C. Liu, X. Luan, Y.-F. Xiao, and C. W. Wong, **Phys. Rev. Lett.** 110, 153606 (2013);
16. “Aluminum nitride piezo-acousto-photonic crystal nanocavity with high quality factors”, L.R. Fan, X. K. Sun, C. Xiong, C. Schuck, H. X. Tang, **Applied Physics Letters**, 102, 153507 (2013)
17. “Photonic crystal dumbbell resonators in silicon and aluminum nitride integrated optical circuits”, W. P. H. Pernice, C. Xiong, H. X. Tang, **Journal of Nanophotonics**, 7, 073095 (2013)
18. “Feedback and harmonic locking of slot-type optomechanical oscillators to external low-noise reference clocks”, J. Zheng, Y. Li, N. Goldberg, M. McDonald, A. Hati, M. Lu, S. Strauf, T. Zhevinsky, D. A. Howe, and C. W. Wong, **Appl. Phys. Lett.** 102, 141117 (2013).
19. “Nonlinear optical response of wavelength-sized ultrahigh-Q silicon disk cavities immersed in superfluid helium”, X. K. Sun, X. F. Zhang, C. Schuck, H. X. Tang, **Scientific Reports** 3, 1436 (2013).
20. “Casimir microscope based upon metallized high Q SiN nanomembrane resonator”, D. Garcia-Sanchez, K. Y. Fong, H. Bhaskaran, S. K. Lamoreaux, H. X. Tang, **Rev. Sci. Instr.** 84, 015115 (2013)

21. "Piezo-optomechanics: piezoelectrically excited, optically sensed nanomechanical resonators", C. Xiong, L. R. Fan, X. K. Sun, H. X. Tang, **Applied Physics Letters** 102, 021110 (2013).
22. "A superhigh-frequency optoelectromechanical system based on a slotted photonic crystal cavity", X. K. Sun, X. F. Zhang, M. Poot, C. Xiong, H. X. Tang, **Appl. Phys. Lett.** 101, 221116 (2012)
23. "Femtogram dispersive L3-nanobeam optomechanical cavities: design and experimental comparison", J. J. Zheng, X. K. Sun, Y. Li, M. Poot, A. Dadgar, N. N. Shi, W.P.H. Pernice, H. X. Tang, and C. W. Wong, **Optics Express** 20, 26486 (2012).
24. "Backaction limits on self-sustained optomechanical oscillators", M. Poot, K. Y. Fong, M. Bagheri, W. P. H. Pernice, H. X. Tang, **Phys. Rev. A** 86, 053826 (2012)
25. "Aluminum Nitride as a new material for chip-scale optomechanics and nonlinear optics", C. Xiong, W. H. P. Pernice, X. K. Sun, C. Schuck, K. Y. Fong, H. X. Tang, **New J. Physics** 14, 095014 (2012).
26. "A 1.16- μ m-radius disk cavity in a sunflower-type circular photonic crystal with ultrahigh quality factor", X. F. Zhang, X. K. Sun, H. X. Tang, **Optics Letters** 15, 3195 (2012)
27. "Casimir force and in-situ surface potential measurements on nanomembranes", D. Garcia-Sanchez, K.Y. Fong, H. Bhaskaran, S.K.Lamoreaux, H. X. Tang, **Phys. Rev. Lett** 109, 027202 (2012)
28. "Low-loss, silicon integrated, aluminum nitride photonic circuits and their use for electro-optic signal processing", C. Xiong, W. H. P. Pernice, H. X. Tang, **Nano Letters** 12, 3562 (2012)
29. "High Q micro-ring resonators fabricated from polycrystalline aluminum nitride films for near infrared and visible photonics", W. H. P. Pernice, C. Xiong, H. X. Tang, **Optics Express** 20, 12261 (2012)
30. "Integrated high frequency aluminum nitride optomechanical resonators", C. Xiong, X.K. Sun, K.Y. Fong, H. X. Tang, **Appl. Phys. Lett.** 100, 171111 (2012)
31. "Observation of KBT/f frequency noise in ultrahigh Q silicon nitride nanomechanical resonators", K. Y. Fong, W. H. P. Pernice, H. X. Tang, **IEEE International Frequency Control Symposium**, 10.1109/FCS.2012.6243678 (2012)
32. "GHz aluminum nitride optomechanical wheel resonators", C. Xiong, X. K. Sun, K. Y. Fong, H. X. Tang, **IEEE International Frequency Control Symposium**, 10.1109/FCS.2012.6243664 (2012)
33. "Frequency and phase noise of ultra-high Q silicon nitride nanomechanical resonators", K. Y. Fong, W. H. P. Pernice, H. X. Tang, **Physical Review B** 85, 161410R (2012)
34. "High-Q silicon optomechanical microdisk resonators at gigahertz frequencies", X. K. Sun, X. F. Zhang, H. X. Tang, **Appl. Phys. Lett.** 100, 173116 (2012)
35. "Femtogram Doubly Clamped Nanomechanical Resonator Embedded in a High-Q Two-Dimensional Photonic Crystal Nanocavity", X. K. Sun, J.J. Zheng, M. Poot, C. W. Wong, H.X. Tang, **Nano Letters** 12, 2299 (2012)
36. W. H. P. Pernice, C. Xiong, C. Schuck, H.X. Tang, "High-Q aluminum nitride photonic crystal nanobeam cavities", **Appl. Phys. Lett.** 100, 091105 (2012)
37. "High-reflectivity, high-Q nanomembrane resonators via guided photonic crystal resonances for enhanced optomechanical coupling", C. Bui*, J. Zheng*, S. W. Hoch, L. Y. T. Lee, J. G. E. Harris, and C. W. Wong, **Appl. Phys. Lett.** 100, 021110 (2012).
38. "Parametric optomechanical oscillations in two-dimensional slot-type high-Q photonic crystal cavities", Jiangjun Zheng, Ying Li, M. S. Aras, A. Stein, K.L. Shepard and C. W. Wong, **Appl. Phys. Lett.** 100, 211908 (2012).
39. "Dynamic manipulation of discrete mechanical states through backaction cooling and amplification", M. Bagheri, M. Li, W. P. H. Pernice, M. Poot, H. X. Tang, **Nature Nanotechnology** 6, 726 (2011)
40. "High-Q-factor GHz optomechanical resonators with high mechanical Q in air", X.K. Sun, K.Y. Fong, C. Xiong, W. P. H. Pernice and H. X. Tang, **Optics Express** 19, 22316 (2011)

41. “Tunable optical coupler controlled by optical gradient forces”, K. Y. Fong, W. P. H. Pernice, M. Li, H. X. Tang, **Optics Express** 19, 015098 (2011)
42. “Carrier and thermal dynamics of silicon photonic resonators at cryogenic temperatures”, W. H. P. Pernice, C. Schuck, M. Li, H. X. Tang, **Optics Express** 19, 3290 (2011)
43. “Ultrahigh-Frequency Nano-Optomechanical Resonators in Slot Ring Cavities”, Mo Li, W. P. H. Pernice, H. X. Tang, **Applied Physics Letters** 97, 183110 (2010)
44. “High performance nanophotonic circuits based on partially buried horizontal slot waveguides”, C. Xiong, W. P. H. Pernice, M. Li, H. X. Tang, **Optics Express** 18, 20690 (2010)
45. “Design of dispersive optomechanical coupling and cooling in ultrahigh-Q/V slot-type photonic crystal cavities”, Y Li, J Zheng, J Gao, J Shu, MS Aras, CW Wong, **Optics Express** 18, 23844 (2010).
46. “Time-domain measurement of optical transport in silicon micro-ring resonators”, W. P. H. Pernice, M. Li, H. X. Tang, **Optics Express** 18, 18438 (2010)
47. “High Q optomechanical resonators in silicon nitride nanophotonic circuits”, K. Y. Fong, W. H. P. Pernice, Mo Li, H. X. Tang, **Applied Physics Letters** 97, 073112 (2010)
48. “Adiabatic embedment of nanomechanical resonators in photonic microring cavities”, C. Xiong, W. H. P. Pernice, Mo Li, M. Rooks, H. X. Tang, **Applied Physics Letters** 96, 263101 (2010)

Appendix 2. Supported postdoc/graduate students

1. Mo Li, Yale postdoc, now Associate Professor of Electrical Engineering, Univ. Minnesota
2. Wolfram Pernice, Yale postdoc, now Professor of Electrical Engineering, Karlsruhe Institute of Technology
3. Mahmood Bagheri, Yale postdoc, now Research Scientist, JPL
4. Harish Bhaskaran, Yale postdoc, now Associate Professor of Material Science and Engineering, Oxford University
5. Daniel Garcia-Sanchez, Yale postdoc, now Junior Group Leader, Institute of Nanoscience, Paris
6. Xiankai Sun, Yale postdoc, now Assistant Professor of Electrical Engineering, Chinese University of Hong Kong.
7. Jiangjun Zheng, Columbia postdoc, now Senior Engineer at Brion Technologies
8. Jing Shu, Columbia postdoc, now Associate Professor, Nanjing University of Science and Technology.
9. Chi Xiong, Yale graduate student, now postdoc at IBM
10. King Yan Fong, Yale graduate student, now postdoc at UC Berkeley
11. Yongchun Liu, Columbia visiting graduate student, now graduate student at Peking University
12. Menno Poot, current postdoc at Yale University
13. Linran Fan, current graduate student at Yale University
14. Xu Han, current graduate student at Yale University
15. Yongjun Huang, current graduate student at UCLA
16. Ying Li, current graduate student at Columbia University

Appendix 3. Honors received by supported postdoc/graduate students

1. Xiankai Sun, Finalist for the Blavatnik Awards for Young Scientist, \$10,000 prize
2. Chi Xiong, Chinese Government Award for Outstanding Students Studying Aboard
3. Chi Xiong, Best Student Paper award, IEEE Frequency Control Symposium
4. King Yan Fong, Best Student Paper Award, IEEE Frequency Control Symposium
5. Menno Poot, Rubicon Fellowship
6. Wolfram Pernice, Emmy Noether Programm awardee and Humboldt foundation fellowship
7. Daniel Garcia, Marie Curie Fellowship
8. Ying Li, SPIE Optics and Photonics Scholarship

AFOSR Deliverables Submission Survey

Response ID:4773 Data

1.

1. Report Type

Final Report

Primary Contact E-mail

Contact email if there is a problem with the report.

hong.tang@yale.edu

Primary Contact Phone Number

Contact phone number if there is a problem with the report

2034324256

Organization / Institution name

Yale University

Grant/Contract Title

The full title of the funded effort.

Circuit cavity optomechanics for cooling and amplification on a silicon chip

Grant/Contract Number

AFOSR assigned control number. It must begin with "FA9550" or "F49620" or "FA2386".

FA9550-10-1-0297

Principal Investigator Name

The full name of the principal investigator on the grant or contract.

Hong Tang

Program Manager

The AFOSR Program Manager currently assigned to the award

Tatjana Curcic.

Reporting Period Start Date

06/15/2010

Reporting Period End Date

06/14/2015

Abstract

In this DARPA's ORCHID program, Yale/Columbia's team focuses on chip-scale optomechanics with emphasis on circuit integration on silicon platforms.

In Phase I (06/2010-06/2012), we advanced the-state-of-art cavity optomechanical devices with performance parameters exceeding DARPA's specifications. Selected high performance devices are optimized for specific applications: (1) low-noise optomechanical oscillators; (2) femtogram optomechanical cavities for sensing; (3) strong optomechanical backaction and coherent control for quantum transducers.

In Phase II (07/2012-06/2015), we added electronic control in Cavity Optomechanics and developed a number of cavity

DISTRIBUTION A: Distribution approved for public release.

electro-optomechanical systems for realizing strong coupling between photon, phonon and microwave fields. These cavity electro-optomechanical systems were fabricated from three different material systems – Si, SiN and AlN. The latter two substrate systems were first designed by our team and now become very popular in Optomechanics community. Particular to the silicon platform, we developed a post-CMOS process which allowed the interrogation of Optomechanics on a CMOS platform with integrated Germanium detectors. The most notable accomplishments we have made in Phase II include: (1) The development of AlN-on-silicon platform for cavity electro-optomechanics and nonlinear optics; (2) Development of X-band optomechanical oscillators; (3) Discovery of phonon "radiation pressure" in optomechanical resonators; (4) Demonstration of coherent control of cavity electro-mechanical resonators; (5) Non-volatile optomechanical switches and memory; (6) Photonic synchronization of two coupled resonators.

Distribution Statement

This is block 12 on the SF298 form.

Distribution A - Approved for Public Release

Explanation for Distribution Statement

If this is not approved for public release, please provide a short explanation. E.g., contains proprietary information.

SF298 Form

Please attach your [SF298](#) form. A blank SF298 can be found [here](#). Please do not password protect or secure the PDF. The maximum file size for an SF298 is 50MB.

[AFD-070820-035.pdf](#)

Upload the Report Document. File must be a PDF. Please do not password protect or secure the PDF. The maximum file size for the Report Document is 50MB.

[Orchid final report 3.pdf](#)

Upload a Report Document, if any. The maximum file size for the Report Document is 50MB.

Archival Publications (published) during reporting period:

1. "Nano-optomechanical resonators in microfluidics", K. Y. Fong, M. Poot, H. X. Tang, Nano Letters, submitted.
2. "A 10-GHz film-thickness-mode cavity optomechanical resonator", X. Han, K. Y. Fong, H. X. Tang, Applied Physics Letters, 106, 161108 (2015)
3. "Deep feedback-stabilized parametric squeezing in an opto-electromechanical system", M. Poot, K. Y. Fong, H. X. Tang, New J. Physics, 17, 043056 (2015)
4. "Cascaded optical transparency in multimode-cavity optomechanical systems", L. R. Fan, K. Y. Fong, M. Poot, H. X. Tang, Nature Communications 6, 5850 (2015)
5. "Coupled cavities for motional ground-state cooling and strong optomechanical coupling", Y.C. Liu, Y.F. Xiao, X.S. Luan, Q.H. Gong and C. W. Wong, Phys. Rev. A 91, 033818.
6. "Classical non-Gaussian state preparation through squeezing in an optoelectromechanical resonator", M. Poot, H. X. Tang, Phys. Rev. A 90, 063809 (2014)
7. "Microwave assisted optical amplification and coherent absorption in cavity piezo-optomechanical system", K. Y. Fong, L. R. Fan, L. Jiang, H. X. Tang, Physical Review A 90, 051801R, 2014
8. "An integrated low phase noise radiation-pressure-driven optomechanical oscillator chipset", X. Luan, Y. Huang, Y. Li, J. F. McMillan, J. Zheng, S.-W. Huang, P.-C. Hsieh, T. Gu, D. Wang, A. Hati, D. A. Howe, G. Wen, M. Yu, G. Lo, D.-L. Kwong, and C. W. Wong, Scientific Reports 4, 6842 (2014);
9. "Phase noise of self-sustained optomechanical oscillators", K. Y. Fong, M. Poot, X. Han, H. X. Tang, Physical Review A 90, 023825 (2014)
10. "The prospect of detecting single-photon force effects in cavity optomechanics", H. X. Tang, and D. Vitali, Physical Review A 89, 063821 (2014)
11. "Triply resonant cavity piezo-optomechanics at X-band", X. Han, C. Xiong, K. Y. Fong, X. F. Zhang, H. X. Tang, New Journal of Physics 16, 063060 (2014).
12. "Monolithically integrated, ultrahigh-frequency cavity nanooptoelectromechanical system with on-chip germanium

DISTRIBUTION A: Distribution approved for public release.

- waveguide photodetector", X. K. Sun, K. Xu, H. X. Tang, Optics Letters 39, 2514 (2014)
13. "Broadband nanoelectromechanical phase shifting of light on a chip", M. Poot, H. X. Tang, Applied Physics Letters 104, 061101 (2014)
14. "Photonic cavity synchronization of nanomechanical oscillators", M. Bagheri, M. Poot, L.R. Fan, F. Marquardt, H. X. Tang, Physical Review Letters 111, 213902 (2013)
15. "Dynamic dissipative cooling of a mechanical oscillator in strong-coupling optomechanics", Y.-C. Liu, X. Luan, Y.-F. Xiao, and C. W. Wong, Phys. Rev. Lett. 110, 153606 (2013);
16. "Aluminum nitride piezo-acousto-photonic crystal nanocavity with high quality factors", L.R. Fan, X. K. Sun, C. Xiong, C. Schuck, H. X. Tang, Applied Physics Letters, 102, 153507 (2013)
17. "Photonic crystal dumbbell resonators in silicon and aluminum nitride integrated optical circuits", W. P. H. Pernice, C. Xiong, H. X. Tang, Journal of Nanophotonics, 7, 073095 (2013)
18. "Feedback and harmonic locking of slot-type optomechanical oscillators to external low-noise reference clocks", J. Zheng, Y. Li, N. Goldberg, M. McDonald, A. Hati, M. Lu, S. Strauf, T. Zelevinsky, D. A. Howe, and C. W. Wong, Appl. Phys. Lett. 102, 141117 (2013).
19. "Nonlinear optical response of wavelength-sized ultrahigh-Q silicon disk cavities immersed in superfluid helium", X. K. Sun, X. F. Zhang, C. Schuck, H. X. Tang, Scientific Reports 3, 1436 (2013).
20. "Casimir microscope based upon metallized high Q SiN nanomembrane resonator", D. Garcia-Sanchez, K. Y. Fong, H. Bhaskaran, S. K. Lamoreaux, H. X. Tang, Rev. Sci. Instr. 84, 015115 (2013)
21. "Piezo-optomechanics: piezoelectrically excited, optically sensed nanomechanical resonators", C. Xiong, L. R. Fan, X. K. Sun, H. X. Tang, Applied Physics Letters 102, 021110 (2013).
22. "A superhigh-frequency optoelectromechanical system based on a slotted photonic crystal cavity", X. K. Sun, X. F. Zhang, M. Poot, C. Xiong, H. X. Tang, Appl. Phys. Lett. 101, 221116 (2012)
23. "Femtogram dispersive L3-nanobeam optomechanical cavities: design and experimental comparison", J. J. Zheng, X. K. Sun, Y. Li, M. Poot, A. Dadgar, N. N. Shi, W.P.H. Pernice, H. X. Tang, and C. W. Wong, Optics Express 20, 26486 (2012).
24. "Backaction limits on self-sustained optomechanical oscillators", M. Poot, K. Y. Fong, M. Bagheri, W. P. H. Pernice, H. X. Tang, Phys. Rev. A 86, 053826 (2012)
25. "Aluminum Nitride as a new material for chip-scale optomechanics and nonlinear optics", C. Xiong, W. H. P. Pernice, X. K. Sun, C. Schuck, K. Y. Fong, H. X. Tang, New J. Physics 14, 095014 (2012).
26. "A 1.16- μm -radius disk cavity in a sunflower-type circular photonic crystal with ultrahigh quality factor", X. F. Zhang, X. K. Sun, H. X. Tang, Optics Letters 15, 3195 (2012)
27. "Casimir force and in-situ surface potential measurements on nanomembranes", D. Garcia-Sanchez, K.Y. Fong, H. Bhaskaran, S.K.Lamoreaux, H. X. Tang, Phys. Rev. Lett 109, 027202 (2012)
28. "Low-loss, silicon integrated, aluminum nitride photonic circuits and their use for electro-optic signal processing", C. Xiong, W. H. P. Pernice, H. X. Tang, Nano Letters 12, 3562 (2012)
29. "High Q micro-ring resonators fabricated from polycrystalline aluminum nitride films for near infrared and visible photonics", W. H. P. Pernice, C. Xiong, H. X. Tang, Optics Express 20, 12261 (2012)
30. "Integrated high frequency aluminum nitride optomechanical resonators", C. Xiong, X.K. Sun, K.Y. Fong, H. X. Tang, Appl. Phys. Lett. 100, 171111 (2012)
31. "Observation of KBT/f frequency noise in ultrahigh Q silicon nitride nanomechanical resonators", K. Y. Fong, W. H. P. Pernice, H. X. Tang, IEEE International Frequency Control Symposium, 10.1109/FCS.2012.6243678 (2012)
32. "GHz aluminum nitride optomechanical wheel resonators", C. Xiong, X. K. Sun, K. Y. Fong, H. X. Tang, IEEE International Frequency Control Symposium, 10.1109/FCS.2012.6243664 (2012)
33. "Frequency and phase noise of ultra-high Q silicon nitride nanomechanical resonators", K. Y. Fong, W. H. P. Pernice, H. X. Tang, Physical Review B 85, 161410R (2012)
34. "High-Q silicon optomechanical microdisk resonators at gigahertz frequencies", X. K. Sun, X. F. Zhang, H. X. Tang, Appl. Phys. Lett. 100, 173116 (2012)
35. "Femtogram Doubly Clamped Nanomechanical Resonator Embedded in a High-Q Two-Dimensional Photonic Crystal Nanocavity", X. K. Sun, J.J. Zheng, M. Poot, C. W. Wong, H.X. Tang, Nano Letters 12, 2299 (2012)
36. W. H. P. Pernice, C. Xiong, C. Schuck, H.X. Tang, "High-Q aluminum nitride photonic crystal nanobeam cavities", Appl. Phys. Lett. 100, 091105 (2012)
37. "High-reflectivity, high-Q nanomembrane resonators via guided photonic crystal resonances for enhanced optomechanical coupling", C. Bui*, J. Zheng*, S. W. Hoch, L. Y. T. Lee, J. G. E. Harris, and C. W. Wong, Appl. Phys. Lett. 100, 021110 (2012).

38. "Parametric optomechanical oscillations in two-dimensional slot-type high-Q photonic crystal cavities", Jiangjun Zheng, Ying Li, M. S. Aras, A. Stein, K.L. Shepard and C. W. Wong, Appl. Phys. Lett. 100, 211908 (2012).
39. "Dynamic manipulation of discrete mechanical states through backaction cooling and amplification", M. Bagheri, M. Li, W. P. H. Pernice, M. Poot, H. X. Tang, Nature Nanotechnology 6, 726 (2011)
40. "High-Q-factor GHz optomechanical resonators with high mechanical Q in air", X.K. Sun, K.Y. Fong, C. Xiong, W. P. H. Pernice and H. X. Tang, Optics Express 19, 22316 (2011)
41. "Tunable optical coupler controlled by optical gradient forces", K. Y. Fong, W. P. H. Pernice, M. Li, H. X. Tang , Optics Express 19, 015098 (2011)
42. "Carrier and thermal dynamics of silicon photonic resonators at cryogenic temperatures", W. H. P. Pernice, C. Schuck, M. Li, H. X. Tang, Optics Express 19, 3290 (2011)
43. "Ultrahigh-Frequency Nano-Optomechanical Resonators in Slot Ring Cavities", Mo Li, W. P. H. Pernice, H. X. Tang, Applied Physics Letters 97, 183110 (2010)
44. "High performance nanophotonic circuits based on partially buried horizontal slot waveguides", C. Xiong, W. P. H. Pernice, M. Li, H. X. Tang, Optics Express 18, 20690 (2010)
45. "Design of dispersive optomechanical coupling and cooling in ultrahigh-Q/V slot-type photonic crystal cavities", Y Li, J Zheng, J Gao, J Shu, MS Aras, CW Wong, Optics Express 18, 23844 (2010).
46. "Time-domain measurement of optical transport in silicon micro-ring resonators", W. P. H. Pernice, M. Li, H. X. Tang, Optics Express 18, 18438 (2010)
47. "High Q optomechanical resonators in silicon nitride nanophotonic circuits", K. Y. Fong, W. H. P. Pernice, Mo Li, H. X. Tang, Applied Physics Letters 97, 073112 (2010)
48. "Adiabatic embedment of nanomechanical resonators in photonic microring cavities", C. Xiong, W. H. P. Pernice, Mo Li, M. Rooks, H. X. Tang, Applied Physics Letters 96, 263101 (2010)

Changes in research objectives (if any):

Change in AFOSR Program Manager, if any:

Extensions granted or milestones slipped, if any:

No cost extension - 1 year from June 15, 2014 to June 14, 2015

AFOSR LRIR Number

LRIR Title

Reporting Period

Laboratory Task Manager

Program Officer

Research Objectives

Technical Summary

Funding Summary by Cost Category (by FY, \$K)

	Starting FY	FY+1	FY+2
Salary			
Equipment/Facilities			
Supplies			
Total			

Report Document

Report Document - Text Analysis

Report Document - Text Analysis

Appendix Documents

2. Thank You

E-mail user

Jul 16, 2015 23:29:17 Success: Email Sent to: hong.tang@yale.edu
